NASA Technical Memorandum 108801

Shake Test Results of the MDHC Test Stand in the 40- by 80-Foot Wind Tunnel

Benton H. Lau and Randall Peterson

January 1994

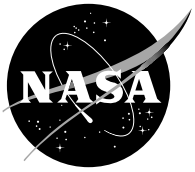

National Aeronautics and
Space Administration

NASA Technical Memorandum 108801

Shake Test Results of the MDHC Test Stand in the 40- by 80-Foot Wind Tunnel

Benton Lau and Randall Peterson, Ames Research Center, Moffett Field, California

January 1994

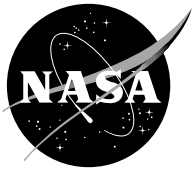

National Aeronautics and
Space Administration

Ames Research Center
Moffett Field, California 94035-1000

Shake Test Results of the MDHC Test Stand in the 40- by 80-Foot Wind Tunnel

BENTON H. LAU AND RANDALL PETERSON

Ames Research Center

Summary

A shake test was conducted to determine the modal properties of the MDHC (McDonnell Douglas Helicopter Company) test stand installed in the 40- by 80-Foot Wind Tunnel at Ames Research Center. The shake test was conducted for three wind-tunnel balance configurations with and without balance dampers, and with the snubber engagement to lock the balance frame. A hydraulic shaker was used to apply random excitation at the rotor hub in the longitudinal and lateral directions. A GenRad 2515 computer-aided test system computed the frequency response functions at the rotor hub and support struts. From these response functions, the modal properties, including the natural frequency, damping ratio, and mode shape were calculated. The critical modes with low damping ratios are identified as the test-stand second longitudinal mode for the dampers-off configuration, the test-stand yaw mode for the dampers-on configuration, and the test-stand first longitudinal mode for the balance-frame locked configuration.

Introduction

In the summer of 1989, McDonnell Douglas Helicopter Company, Bell Helicopter Textron Inc., and NASA jointly conducted the Light Helicopter Experimental (LHX) test in the 40- by 80-Foot Wind Tunnel at NASA Ames Research Center. Upon installation of the MDHC test stand and a 1/2-scale LHX fuselage model in the wind tunnel, a shake test was conducted to obtain the frequency response functions at the rotor hub and at the wind-tunnel support struts. The shake test results would be used in a stability analysis to determine the potential of rotor instability because a primary safety concern in rotor testing is the prevention of ground resonance instability. Instability can occur when the rotor damping is insufficient and when the frequencies of the rotor and the test support system coalesce. The occurrence of instability can endanger test personnel and severely damage the rotor and test facility. This report describes the test setup, test procedures, data reduction, and results.

Nomenclature

A	residue, g·rad/(lb·s)
C	modal damping coefficient, lb·s/ft
G	gravitational constant, 32.2 ft/(g·s^2)
K	modal stiffness, lb/ft
M	modal mass, slug
ζ	damping ratio
ω	natural frequency, rad/s

Subscript

r	rth structural mode

Mechanical System

The mechanical system included the MDHC test stand, the LHX fuselage model, the 600-hp electric motor, and the gear box. The test stand consisting of the main strut, the horizontal support strut, and the sled, was supported by two front struts (2 ft struts with 60 inch tips) and a tail strut. The fuselage was installed on the main strut; the motor and the gear box were mounted on the sled. Figure 1 shows the mechanical system and the test set up for longitudinal excitation. The rotor balance and the fuselage balance were enclosed in the fuselage. These balances provided accurate measurements of the rotor and fuselage loads. Only the rotor balance responses were measured in the shake test. A dummy hub with equivalent weight of the actual hub plus half the total weight of the blades was used in the shake test. The test-stand angle of attack and yaw angle were set at zero degree, and fairings of the main strut and the sled were removed. The effects of these fairings on the shake test results were assumed insignificant because of the distant locations among the fairings and the hub and their light weights in comparison to the total weight of test stand.

Shaker System

The shaker system consisted of the MTS Model 406.11 shaker controller and the Model 204.08 hydraulic actuator. The shaker controller operated the actuator in stroke

feedback mode. One end of the actuator was attached to a 11,600 lb reaction mass and the other end to the dummy hub (see fig. 1). A load cell placed between the actuator and the hub measured the shaker force. A 5-ft extension beam was placed between the actuator and the reaction mass to maintain the excitation force being applied along the main axis of the load cell. Additionally, the extension beam provided spacing between the reaction mass and the model.

Test Configurations

The test stand was supported by two front struts and a tail support strut and installed on the wind-tunnel balance. Since the wind-tunnel balance was designed to measure the total forces and moments acting on the test model, the balance provides very little damping. Hydraulic dampers, however, can be attached to the balance for additional damping. If the balance is not used in testing, a set of snubbers are engaged to lock the balance frame motion.

All three balance configurations (dampers off, dampers on, and locked) were tested in the shake test. For each configuration, the longitudinal (fore and aft) and lateral (side to side) excitations were applied at the rotor hub.

Instrumentation and Data Acquisition

Eight accelerometers, one load cell, and four rotor-balance channels were used during the shake test. The load cell was calibrated to measure up to ±1000 lb. The accelerometers were calibrated to ±1 g with a frequency range between zero and 100 Hz. One pair of accelerometers measured the longitudinal and lateral responses at the center of the rotor hub, and three pairs of accelerometers measured the longitudinal and lateral responses at the two front struts and at the tail strut. The accelerometers were mounted at nodes 1, 3, 4, and 8 on the stick model representation shown in figure 2. Table 1 lists the nodal coordinates of the stick model. The rotor-balance channels measured in the shake test include the axial force, the side force, and the pitching and rolling moments. Positive directions of the balance channels are shown in figure 2. Broadband random excitation was used in the test. The excitation level were in the order of ±100 lb for lateral excitation and ±190 lb for longitudinal excitation.

All data were acquired on a GenRad 2515 computer aided test system. The GenRad system is capable of acquiring 16 channels of data and displaying in two screens simultaneously. The system computed and stored the frequency response functions on a hard disk. The functions were then transferred to a Micro VAX II workstation for off-line data processing.

Table 1. Nodal coordinates of the test-stand stick model. Origin of the coordinate system is at midpoint between nodes 5 and 6

	Coordinate (inch)		
Node	X	Y	Z
1	0.0	0.0	268.0
2	0.0	0.0	84.0
3	0.0	48.0	84.0
4	0.0	–48.0	84.0
5	0.0	48.0	0.0
6	0.0	–48.0	0.0
7	0.0	0.0	59.5
8	–98.0	0.0	76.0
9	–74.0	0.0	59.5
10	–98.0	0.0	0.0

The bandwidth of the response functions was set according to the nominal operating speed of the rotor. For the maximum rotor speed of 924 rpm (15.4 Hz), the bandwidth was between zero and 16 Hz for the 1/rev vibration modes and ground resonance, and between zero and 64 Hz for the 4/rev vibration modes. Frequency resolution of both bandwidths was 512 spectral lines. A flat-top window was applied to the data records and fifty records with maximum overlapping were found sufficient for data averaging.

Modal Analysis

The modal analysis was performed on the Micro VAX II workstation using the MODAL-PLUS 9.0 software package (ref. 1). A time-domain curve-fitting algorithm, the Polyreference method, was applied to reduce the test data (ref. 2). The method uses the frequency response data from multiple reference locations in a global least-squares fashion. The method can be divided into three major steps. The first step is to accumulate each response function into a correlation matrix. The next step is to estimate the poles (roots) and damping values from the correlation matrix. The final step is to compute a least-squares estimate of the residues for each resonanent frequency at a response location (ref. 3).

An error chart for the correlation matrix was generated to show the order of error magnitude plotted against the number of estimated roots. The chart assists the user in determining the number of roots in the curve-fitting procedure. Figure 3 shows the error charts of the accelerometer responses in two bandwidths for the dampers-off configuration. A least-squares curve fitting of the residues was then generated for a driving-point response function.

The residues were scaled with the hub longitudinal response for longitudinal excitation and the hub lateral response for lateral excitation. Normal modes were assumed in the residue computation. Table 2 presents the estimated roots of the dampers-off configuration for two bandwidths. Each root includes natural frequency, damping ratio, residue amplitude, phase, and modal confidence factor. Both computational and physical roots are listed in the table. The Modal Confidence Factor (MCF) can be used to assist in differentiating between the computational and the physical modes. The MCF takes on a value near one for physical modes and a value less than one for computational modes (ref. 1, section 6.2.4.1). The last column in table 2 lists the MCF values for each root. The computational roots indicated by "*," however, were suppressed before a synthesized response function was generated. Figure 4 compares the measured hub response functions with the synthesized functions in the longitudinal direction for the dampers-off configuration. Similarly, figure 5 compares the synthesized and the measured hub responses in the lateral direction. Residual corrections were added to the synthesized functions to take into account the vibration modes outside the bandwidth of the analysis (ref. 4). The above procedures were then repeated for the dampers-on and the locked configurations.

Table 2. Natural frequencies, damping ratios, residue amplitudes, phases, and modal confidence factors for the dampers-off configuration

Root no.	Frequency (Hz)	Damping ratio	Residue (g·rad/lb·s)	Phase (rad)	MCF
(a) 1.4 to 5.4 Hz					
1	1.992	0.03375	3.06058E-04	1.571	0.989
2*	1.594	0.43187	5.82778E-04	3.142	0.000
3*	1.914	0.39280	2.04353E-04	1.571	0.017
4	2.458	0.02747	2.50995E-07	–1.571	0.987
5*	2.792	0.03854	1.51837E-04	–1.571	0.981
6	2.804	0.02146	1.24947E-03	1.571	0.998
7*	2.923	0.05460	7.40524E-05	–1.571	0.844
8*	3.844	0.35995	2.83694E-03	–1.571	0.000
9*	4.469	0.14333	1.49897E-03	–1.571	0.013
10*	4.560	0.04082	9.78870E-05	–1.571	0.706
11	4.608	0.01377	1.29118E-07	1.571	0.997
12*	4.636	0.22002	3.52108E-03	1.571	0.001
13*	5.093	0.11067	1.51206E-04	1.571	0.057
14*	5.438	0.00406	5.68810E-05	3.142	0.000
15*	5.438	0.01115	2.23601E-06	0.000	0.000
16*	5.566	0.21403	2.60332E-05	3.142	0.000
(b) 5.4 to 9.5 Hz					
1*	5.408	0.02602	9.15835E-07	3.142	0.000
2*	5.658	0.13002	8.18122E-04	–1.571	0.020
3*	5.511	0.19420	3.79092E-04	0.000	0.000
4	6.781	0.01347	7.50391E-06	–1.571	0.983
5*	6.856	0.01515	1.50743E-06	1.571	0.970
6	7.234	0.01095	4.25937E-04	1.571	0.992
7*	7.364	0.05601	1.04277E-06	–1.571	0.053
8*	7.839	0.02516	6.24227E-05	1.571	0.406
9*	7.887	0.03666	1.10630E-05	–1.571	0.286
10*	8.917	0.07591	7.49061E-05	–1.571	0.054
11	9.204	0.01563	4.04831E-06	1.571	0.999
12*	9.406	0.00317	1.29642E-04	0.000	0.000
13*	9.409	0.02218	2.12085E-05	0.000	0.000
14*	9.552	0.17380	2.37746E-04	3.142	0.000
15*	9.665	0.22964	9.49389E-03	3.142	0.000

*Indicates suppressed roots.

In addition to the MCF values, the Multivariate Mode Indicator method is used to identify the physical modes. The method uses the accelerometer response functions from the longitudinal and lateral reference coordinates to obtain the Mode Indicator Function (MIF) (ref. 1, section 3.3.7). The MIF has a maximum value of unity and a number of local minimums where the modes of the structure exist. Typical MIF plots are shown in figure 6 for three test configurations using a 64-Hz bandwidth. For frequencies below 16 Hz, the MIF plots provide a good estimate of the natural frequencies. However, for structural modes over 20 Hz, estimating the natural frequencies from the MIF plots becomes difficult.

After the roots were obtained, their corresponding mode shapes were calculated. Mode shapes at nodes 1, 3, 4, and 8 (see fig. 2) were computed from the measured response functions. Since the responses at nodes 2, 7, and 9 were not available, these mode shapes could only be estimated from the others. The mode shape at node 2 was linearly interpolated between those at nodes 3 and 4. Similarly, the mode shapes at node 7 was linearly extrapolated between the mode shapes at nodes 1 and 2, and node 9 was linearly interpolated between nodes 7 and 8.

Modal Assurance Criterion (MAC) was used to examine the degree of independence between two mode shapes. MAC has a value from zero (no consistent correspondence) to unity (consistent correspondence). Although not a true orthogonality check with respect to the mass or stiffness matrix, MAC can be used as a measure of the linear independence between two mode shapes.

The modal mass, stiffness, and damping were computed using equations 1–3. The modal mass in equation 1 was scaled with respect to unit mode shape at the hub in either the longitudinal or lateral direction.

$$M_r = \frac{\omega_r}{2G\left|A_r\right|\sqrt{1-\zeta_r^2}} \tag{1}$$

$$K_r = M_r\omega_r^2 \tag{2}$$

$$C_r = 2\zeta_r M_r\omega_r \tag{3}$$

Results and Discussion

Natural frequencies for the three test configurations are listed in table 3. For the dampers-off configuration (table 3a), the longitudinal mode of the balance frame has a fundamental frequency of 1.99 Hz, increasing slightly to 2.32 Hz when dampers are installed (table 3b). When the balance is locked, the test-stand first longitudinal mode becomes the fundamental frequency at 2.48 Hz. All frequencies below 15 Hz were calculated from a modal analysis; frequencies above 15 Hz were estimated from the MIF plots in figure 6. The modal descriptions were selected according to mode shape displays to be discussed later in the report.

Table 3. Natural frequencies of MDHC test stand in the 40-by 80-Foot Wind Tunnel for three test configurations

Mode no.	Frequency (Hz)	Modal description
(a) Dampers off		
1	1.99	Balance frame longitudinal
2	2.46	Balance frame lateral
3	2.80	Test stand 1st longitudinal
4	4.61	Test stand 1st lateral
5	6.78	Test stand yaw
6	7.23	Test stand 2nd longitudinal
7	9.20	Test stand 2nd lateral
8	15.9	—
9	20.5	—
10	22.0	—
11	41.2	—
(b) Dampers on		
1	2.32	Balance frame longitudinal
2	2.76	Test stand 1st longitudinal
3	2.94	Balance frame lateral
4	4.72	Test stand 1st lateral
5	6.79	Test stand yaw
6	7.28	Test stand 2nd longitudinal
7	9.19	Test stand 2nd lateral
8	15.8	—
9	20.0	—
10	21.8	—
(c) Locked		
1	2.48	Test stand 1st longitudinal
2	3.83	Test stand 1st lateral
3	6.69	Test stand yaw
4	9.25	Test stand 2nd lateral
5	15.8	—
6	19.6	—
7	21.7	—
8	43.4	—

The modal properties of the MDHC test stand are listed in table 4 for the three test configurations. These properties include natural frequency, damping ratio, and residue. Among the seven modes analyzed in the dampers-off configuration, the test-stand second longitudinal mode has the lowest damping ratio of 1.10%; installation of dampers improves the damping ratio slightly to 1.42%. Damping ratios of the balance-frame longitudinal and lateral modes,

Table 4. Modal properties of MDHC test stand for three test configurations in the 40-by 80-Foot Wind Tunnel

(a) Dampers off

Modal parameters	Mode 1 Bal. frame longitudinal	Mode 2 Bal. frame lateral	Mode 3 Test-stand 1st longitudinal	Mode 4 Test-stand 1st lateral	Mode 5 Test-stand yaw	Mode 6 Test-stand 2nd longitudinal	Mode 7 Test-stand 2nd lateral
Frequency, Hz	1.992	2.459	2.804	4.608	6.781	7.234	9.204
Damping ratio, %	3.38	2.78	2.15	1.38	1.35	1.10	1.56
Residue, g·rad/(lb·s)	3.0606E – 04	1.4770E – 04	1.2495E – 03	1.3292E – 03	9.1479E – 04	4.2590E – 04	1.5269E – 03
Modal mass, slug	636.16	1626.97	219.27	338.69	724.18	1659.32	588.92
Modal stiffness, lb/ft	9.9656E + 04	3.8838E + 05	6.8060E + 04	2.8391E + 05	1.3146E + 06	3.4281E + 06	1.9695E + 06
Modal damping, lb·s/ft	537.45	1398.64	165.80	270.06	831.22	1651.71	1064.63

(b) Dampers on

Modal parameters	Mode 1 Bal. frame longitudinal	Mode 2 Test-stand 1st longitudinal	Mode 3 Bal. frame lateral	Mode 4 Test-stand 1st lateral	Mode 5 Test-stand yaw	Mode 6 Test-stand 2nd longitudinal	Mode 7 Test-stand 2nd lateral
Frequency, Hz	2.319	2.763	2.935	4.717	6.791	7.280	9.192
Damping ratio, %	6.60	5.04	10.93	4.16	1.21	1.42	1.38
Residue, g·rad/(lb·s)	1.4126E – 03	2.4664E – 04	3.5380E – 04	1.1961E – 03	1.1130E – 03	5.8187E – 04	1.1590E – 03
Modal mass, slug	160.72	1095.73	815.25	385.57	596.10	1222.32	774.85
Modal stiffness, lb/ft	3.4121E + 04	3.3024E + 05	2.7725E + 05	3.3869E + 05	1.0853E + 06	2.5574E + 06	2.5846E + 06
Modal damping, lb·s/ft	308.93	1916.69	3286.18	950.32	612.99	1592.34	1235.14

(c) Locked

Modal parameters	Mode 1 Test-stand 1st longitudinal	Mode 2 Test-stand 1st lateral	Mode 3 Test-stand yaw	Mode 4 Test-stand 2nd lateral
Frequency, Hz	2.476	3.829	6.692	9.252
Damping ratio, %	1.041	1.44	1.90	1.39
Residue, g·rad/(lb·s)	1.1001E – 03	1.0927E – 03	5.7888E – 04	1.0700E – 03
Modal mass, slug	219.87	342.34	1129.5	844.75
Modal stiffness, lb/ft	5.3215E + 04	1.9815E + 05	1.9969E + 06	2.8547E + 06
Modal damping, lb·s/ft	71.22	236.71	1808.48	1369.10

however, increase substantially with damper installation (from 3.38% and 2.78% to 6.60% and 10.93%, respectively). The damping ratios of both test-stand first longitudinal and lateral modes also increase from 2.15% and 1.38% to 5.04% and 4.16%, respectively. The damping ratio of the test-stand yaw mode decreases slightly (from 1.35% to 1.21%) with damper installation, as does the second lateral mode (from 1.56% to 1.38%). In the locked configuration, the most critical mode is the test-stand first longitudinal mode with a very low damping ratio of 1.04%.

Mode shapes and modal assurance criterion matrices are presented in tables 5–7 for the three test configurations. When a mode shape is linearly interpolated between two adjacent mode shapes, the interpolated mode shape is printed in *italics* for ease of identification. Since no response measurement is available at the bases of the support struts (nodes 5, 6, and 10), a value of zero is substituted at these nodes. All mode shapes are scaled with respect to either the hub longitudinal or lateral response.

Mode shape dependence is checked by applying the modal assurance criterion. A MAC value near unity indicates a high degree of correlation between two mode shapes. Section (b) of tables 5–7 list the MAC matrices for each test configuration. A moderate to high degree of dependence is found between the test stand lateral modes and the balance-frame lateral mode. In table 5b, the MAC value between the balance-frame lateral mode and the test stand first lateral mode shows a moderate degree of dependence. This dependence is decreased with the damper installation; however, the dependence between the balance-frame lateral mode and the test-stand second lateral mode is increased. For all three configuration, a moderate level of dependence between the test stand yaw mode and the test-stand second lateral mode exists.

Mode shape displays corresponding to the modal descriptions listed in table 3 for the dampers-off configuration are shown in figure 7. A comparison of the balance-frame modes identified in references 1 and 2 suggests that the natural frequency at 1.99 Hz is the longitudinal mode of the balance-frame as shown in figure 7(a), and the frequency at 2.46 Hz is the lateral mode (fig. 7(b)). A large rotor-hub response at 2.80 Hz (fig. 7(c)) indicates the first longitudinal mode of the test stand. A large response at 4.61 Hz (fig. 7(d)) indicates the first lateral mode of the test stand. The test-stand yaw mode at 6.78 Hz can be identified in figure 7(e). Finally, the modes at 7.23 and 9.20 Hz are identified as the second test-stand longitudinal and lateral modes shown in figures 7(f) and 7(g), respectively. The mode shape displays of the other two test configurations (not shown) are similar to the dampers-off configuration. If responses of the support strut bases (nodes 2, 5, 6, 7, 9, and 10) were recorded, the modal displays in figure 7 would provide more accurate identification of the mode shape.

Table 5. Mode shape and modal assurance criterion check for the dampers-off configuration

(a) Mode shape

Node	Mode 1 Balance frame longitudinal		Mode 2 Balance frame lateral		Mode 3 Test-stand 1st longitudinal		Mode 4 Test-stand 1st lateral	
	X	Y	X	Y	X	Y	X	Y
1	1.0000	0.0516	0.1311	1.0000	1.0000	0.0272	0.0383	1.0000
2	0.4929	–0.0191	0.0847	1.9209	0.0441	–0.0190	–0.0022	0.3921
3	0.4943	–0.0260	–0.0377	1.9375	0.0385	–0.0213	0.1553	0.3929
4	0.4914	–0.0122	0.2072	1.9042	0.0498	–0.0167	–0.1597	0.3912
5	0.0000	0.0000	0.0000	0.0000	0.0000	0.0000	0.0000	0.0000
6	0.0000	0.0000	0.0000	0.0000	0.0000	0.0000	0.0000	0.0000
7	0.4253	–0.0286	0.0785	2.0435	–0.0832	–0.0252	–0.0076	0.3111
8	0.3364	–0.0015	0.0170	1.6964	–0.1917	–0.0336	–0.0165	0.7593
9	0.3581	–0.0081	0.0321	1.7814	–0.1651	–0.0315	–0.0144	0.6495
10	0.0000	0.0000	0.0000	0.0000	0.0000	0.0000	0.0000	0.0000

Node	Mode 5 Test-stand yaw		Mode 6 Test-stand 2nd longitudinal		Mode 7 Test-stand 2nd lateral	
	X	Y	X	Y	X	Y
1	0.1530	1.0000	1.0000	–0.1401	–0.1271	1.0000
2	–0.1829	0.0206	–1.4762	0.0389	0.1863	–0.6799
3	–1.5247	0.0522	–1.3693	0.0520	–0.0055	–0.6747
4	1.1590	–0.0109	–1.5831	0.0257	0.3781	–0.6850
5	0.0000	0.0000	0.0000	0.0000	0.0000	0.0000
6	0.0000	0.0000	0.0000	0.0000	0.0000	0.0000
7	–0.2276	–0.1098	–1.8059	0.0627	0.2281	–0.9035
8	–0.3016	–3.2569	–2.3426	0.2330	0.4112	–1.3666
9	–0.2835	–2.4861	–2.2112	0.1913	0.3663	–1.2532
10	0.0000	0.0000	0.0000	0.0000	0.0000	0.0000

(b) Modal assurance criterion check

Mode	Balance frame lng.	Balance frame lat.	Test-stand 1st lng.	Test-stand 1st lat.	Test-stand yaw	Test-stand 2nd lng.	Test-stand 2nd lat.
Balance frame lng.	1.0000	0.0006	0.3550	0.0002	0.0025	0.2733	0.0267
Balance frame lat.		1.0000	0.0006	0.6813	0.1587	0.0004	0.5262
Test-stand 1st lng.			1.0000	0.0000	0.0100	0.1323	0.0009
Test-stand 1st lat.				1.0000	0.2163	0.0028	0.2160
Test-stand yaw					1.0000	0.0023	0.4881
Test-stand 2nd lng.						1.0000	0.1050
Test-stand 2nd lat.							1.0000

Table 6. Mode shape and modal assurance criterion check for the dampers-on configuration

(a) Mode shape

Node	Mode 1 Balance frame longitudinal		Mode 2 Test-stand 1st longitudinal		Mode 3 Balance frame lateral		Mode 4 Test-stand 1st lateral	
	X	Y	X	Y	X	Y	X	Y
1	1.0000	0.0577	1.0000	–0.0096	–0.5841	1.0000	0.0339	1.0000
2	0.3207	–0.0263	–0.0085	0.1815	0.0136	–1.8475	–0.0023	0.4253
3	0.3207	–0.0315	0.0000	0.1790	–0.1103	–1.8514	0.2003	0.4265
4	0.3208	–0.0212	–0.0169	0.1840	0.1374	–1.8437	–0.2048	0.4240
5	0.0000	0.0000	0.0000	0.0000	0.0000	0.0000	0.0000	0.0000
6	0.0000	0.0000	0.0000	0.0000	0.0000	0.0000	0.0000	0.0000
7	0.2303	–0.0375	–0.1427	0.2070	0.0932	–2.2267	–0.0071	0.3487
8	0.1209	–0.0186	–0.3899	0.1948	0.3328	–2.1736	–0.0138	0.8991
9	0.1476	–0.0232	–0.3294	0.1978	0.2741	–2.1866	–0.0121	0.7644
10	0.0000	0.0000	0.0000	0.0000	0.0000	0.0000	0.0000	0.0000

Node	Mode 5 Test-stand yaw		Mode 6 Test-stand 2nd longitudinal		Mode 7 Test-stand 2nd lateral	
	X	Y	X	Y	X	Y
1	0.1389	1.0000	1.0000	0.1001	–0.1731	1.0000
2	–0.1581	0.0031	–3.8304	0.0035	0.2362	–0.8567
3	–1.3083	0.0298	–3.6560	0.0349	–0.0110	–0.8529
4	0.9922	–0.0235	–4.0047	–0.0280	0.4834	–0.8604
5	0.0000	0.0000	0.0000	0.0000	0.0000	0.0000
6	0.0000	0.0000	0.0000	0.0000	0.0000	0.0000
7	–0.1976	–0.1296	–4.4735	–0.0094	0.2907	–1.1039
8	–0.2623	–2.8119	–6.1083	0.2319	0.5119	–1.7439
9	–0.2464	–2.1550	–5.7079	0.1728	0.4577	–1.5872
10	0.0000	0.0000	0.0000	0.0000	0.0000	0.0000

(b) Modal assurance criterion check

Mode	Balance frame lng.	Test-stand 1st lng.	Balance frame lat.	Test-stand 1st lat.	Test-stand yaw	Test-stand 2nd lng.	Test-stand 2nd lat.
Balance frame lng.	1.0000	0.3286	0.0002	0.0000	0.0001	0.1479	0.0155
Test-stand 1st lng.		1.0000	0.2522	0.0948	0.0184	0.1824	0.2295
Balance frame lat.			1.0000	0.4131	0.3393	0.0088	0.8933
Test-stand 1st lat.				1.0000	0.2601	0.0014	0.3353
Test-stand yaw					1.0000	0.0092	0.5138
Test-stand 2nd lng.						1.0000	0.0765
Test-stand 2nd lat.							1.0000

Table 7. Mode shape and modal assurance criterion check for the locked configuration

(a) Mode shape

Node	Mode 1 Test-stand 1st longitudinal		Mode 2 Test-stand 1st lateral		Mode 3 Test-stand yaw		Mode 4 Test-stand 2nd lateral	
	X	Y	X	Y	X	Y	X	Y
1	1.0000	0.0513	0.0409	1.0000	0.0859	1.0000	–0.1422	1.0000
2	0.2227	–0.0102	0.0057	0.5725	–0.0786	0.0355	0.2224	–0.6922
3	0.2227	–0.0144	0.1015	0.5758	–1.5173	0.0711	0.0434	–0.6915
4	0.2227	–0.0060	–0.0901	0.5692	1.3602	–0.0001	0.4014	–0.6928
5	0.0000	0.0000	0.0000	0.0000	0.0000	0.0000	0.0000	0.0000
6	0.0000	0.0000	0.0000	0.0000	0.0000	0.0000	0.0000	0.0000
7	0.1192	–0.0184	0.0010	0.5156	–0.1005	–0.0929	0.2709	–0.9175
8	0.0123	–0.0055	–0.0153	0.7983	–0.1143	–3.4537	0.4550	–1.3581
9	0.0385	–0.0086	–0.0113	0.7291	–0.1109	–2.6306	0.4099	–1.2502
10	0.0000	0.0000	0.0000	0.0000	0.0000	0.0000	0.0000	0.0000

(b) Modal assurance criterion check

Mode	Test-stand 1st lng.	Test-stand 1st lateral	Test-stand yaw	Test-stand 2nd lateral
Test-stand 1st lng.	1.0000	0.0008	0.0004	0.0033
Test-stand 1st lateral		1.0000	0.1869	0.2889
Test-stand yaw			1.0000	0.4896
Test-stand 2nd lateral				1.0000

Concluding Remarks

A shake test was conducted to determine the modal properties of the MDHC test stand in the 40-by 80-Foot Wind Tunnel. The modal properties were calculated out to 16 Hz for three wind-tunnel balance configurations: dampers-off, dampers-on, and locked. The following remarks are concluded from the test results.

1. Natural frequencies estimated from the MIF plots are very close to those calculated from the modal analysis. The MIF plots indicate highly coupled structural modes in the frequency range above 20 Hz for the three test configurations.

2. In the dampers-off configuration, the second longitudinal mode of the test stand has the lowest damping ratio of 1.10%. When balance dampers are installed, substantial increases in damping are observed in the balance-frame modes and the first modes of the test stand. The test-stand yaw mode has the lowest damping ratio (1.21%) with dampers installed. When the balance frame is locked, the first longitudinal mode of the test stand has the lowest damping ratio (1.04%).

3. In the dampers-off and dampers-on configurations, a moderate to high degree of mode shape dependence is observed between the lateral modes of the balance frame and the test stand. Additional accelerometer measurements would provide more accurate information on the mode shape interdependency.

4. Modal identification can be improved with additional accelerometers measured at the bases of the main strut and the support struts.

References

1. User Manual for MODAL ANALYSIS 9.0. Structural Dynamics Research Corporation, 1985.
2. Vold, H.; Kundrat, J.; Rocklin, G. T.; and Russell, R.: A Multi-input Modal Estimation Algorithm for Mini-computers. SAE Paper Number 820194, 1982.
3. Crowley, S. M.; and Allemang, R. J.: Applications of the Poly Reference Technique in Experimental Modal Analysis. Proceedings of the 2nd International Modal Analysis Conference, Orlando, Florida, 1984.
4. Ewins, D. J.: Modal Testing: Theory and Practice. Research Studies Press Ltd., John Wiley & Sons, Inc.
5. Hoque, M. S.; and Graham, T. A.: Dynamic Characteristics of Bell M412 Pylon and Model 576 Test Stand in the 40- by 80-Foot Wind Tunnel. NASA TM-102880, April 1991.
6. Johnson, W.; and Biggers, J. C.: Shake Test of Rotor Test Apparatus in the 40- By 80-Foot Wind Tunnel. NASA TMX-62418, July 1975.

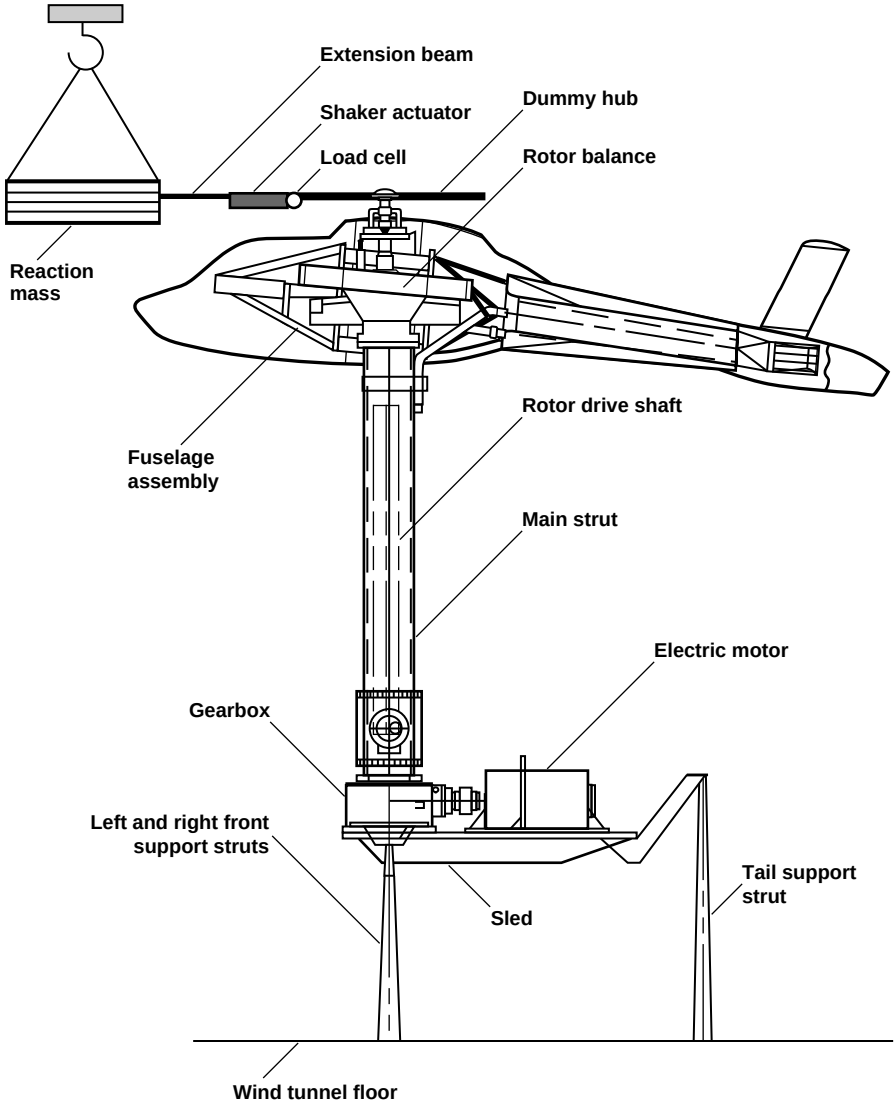

Figure 1. Schematic of MDHC test stand and shake test setup in longitudinal excitation direction in the 40- by 80-Foot Wind Tunnel.

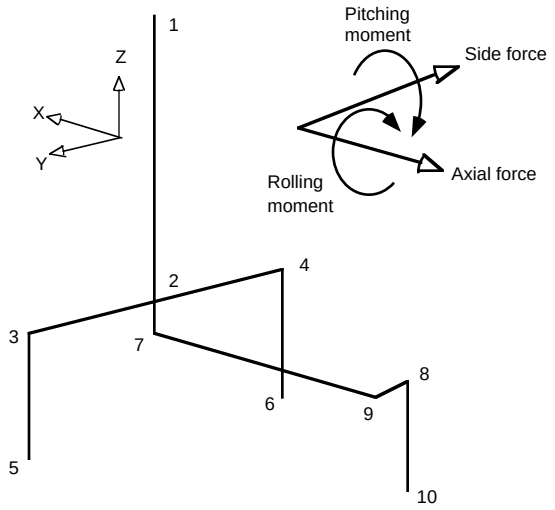

Figure 2. Stick model representation of MDHC test stand and positive directions of rotor balance loads.

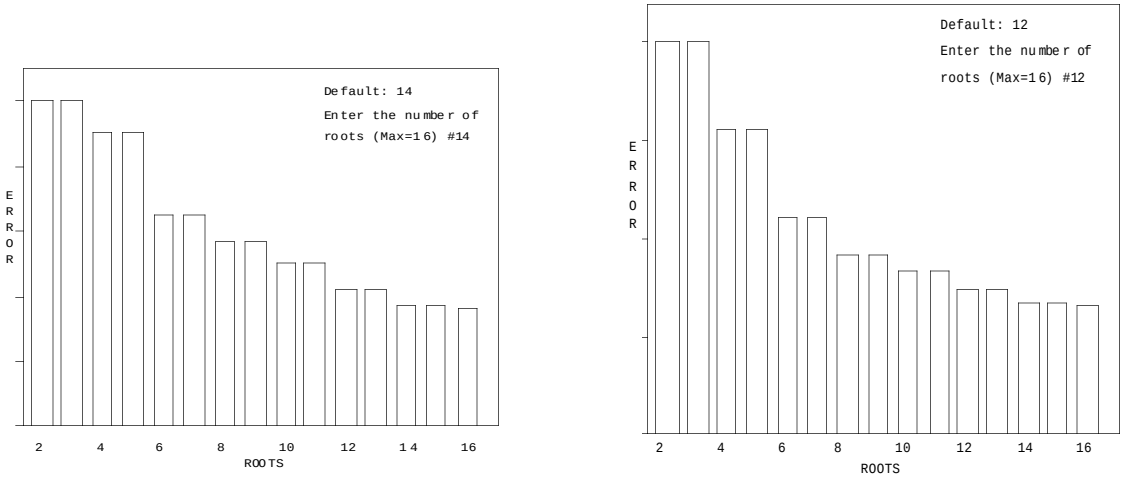

(a) *(b)*

Figure 3. Error charts of accelerometer responses for the dampers-off configuration. (a) 1.4 to 5.4 Hz. (b) 5.4 to 9.4 Hz.

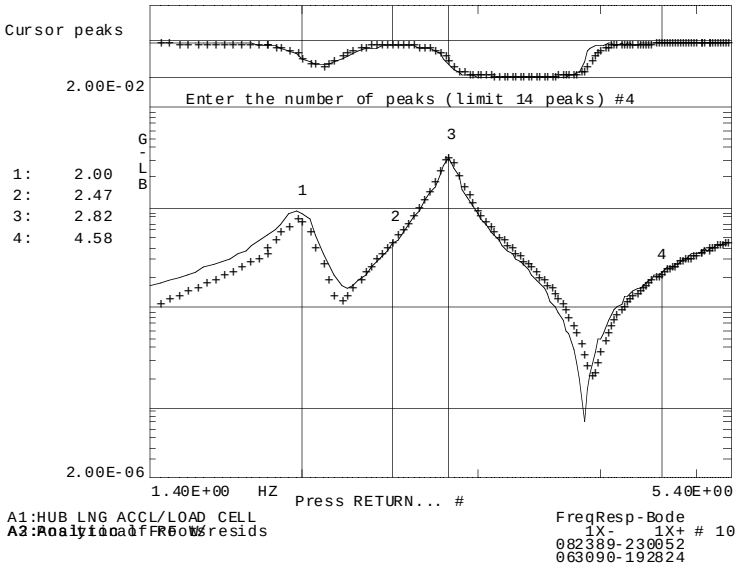

(a)

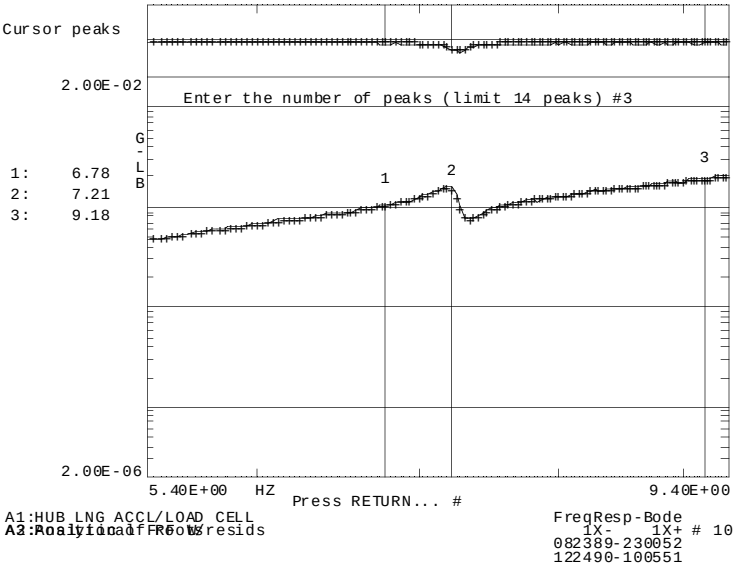

(b)

Figure 4. Comparison of synthesized and measured hub longitudinal responses for the dampers-off configuration. (a) 1.4 to 5.4 Hz. (b) 5.4 to 9.4 Hz.

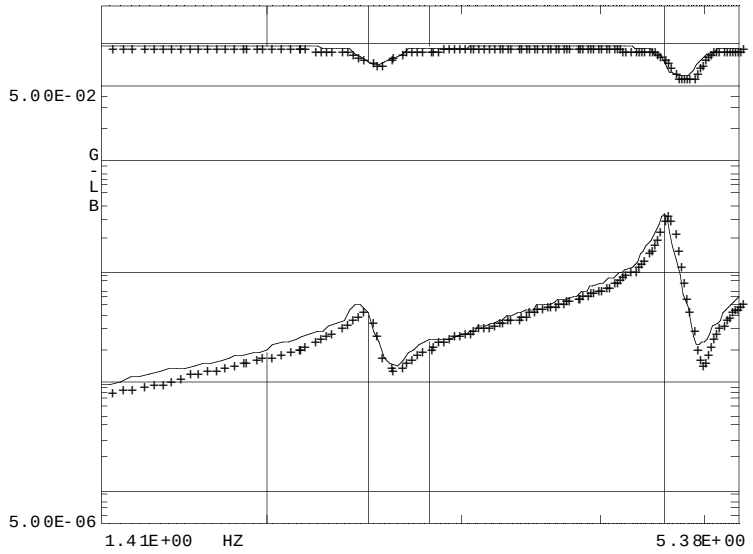

(a)

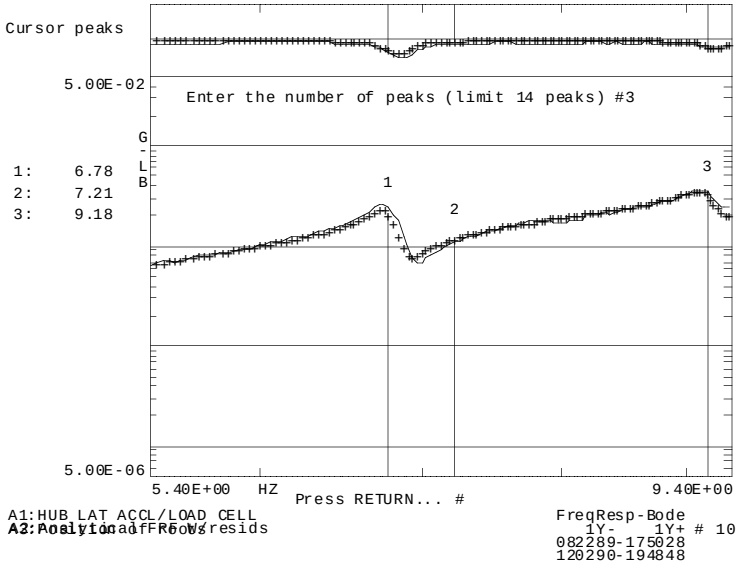

(b)

Figure 5. Comparison of synthesized and measured hub lateral responses for the dampers-off configuration. (a) 1.4 to 5.4 Hz. (b) 5.4 to 9.4 Hz.

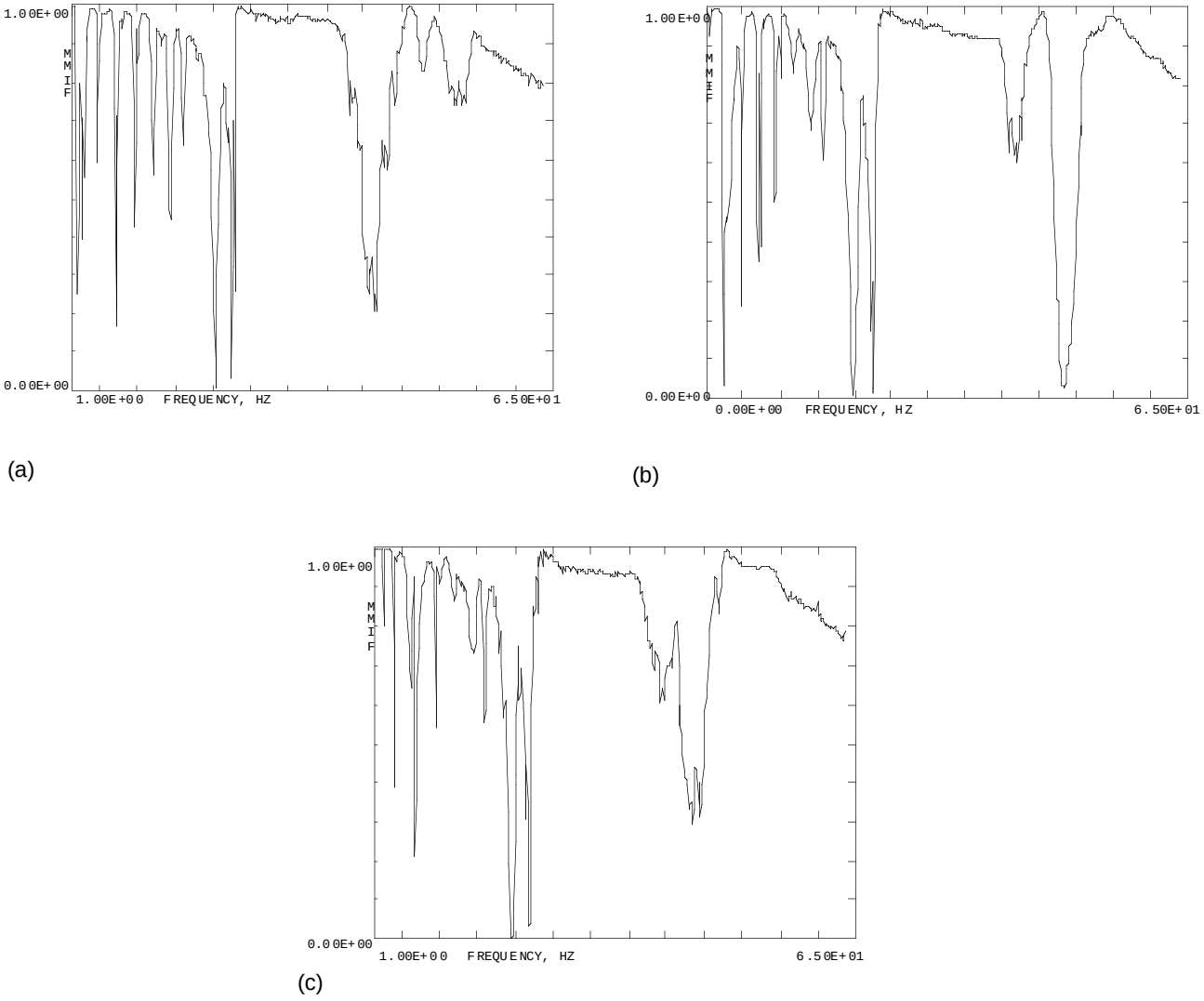

Figure 6. Multivariate Mode Indicator Function (MMIF) plot for three test configurations. (a) Dampers off. (b) Dampers on. (c) Balance frame locked.

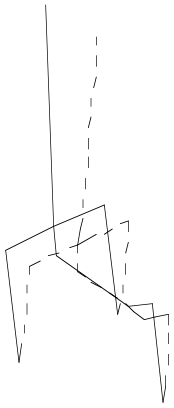

(a) Balance-frame longitudinal mode at 1.99 Hz.

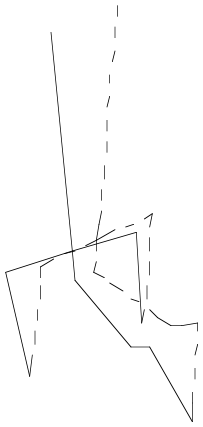

(d) Test-stand 1st lateral mode at 4.61 Hz.

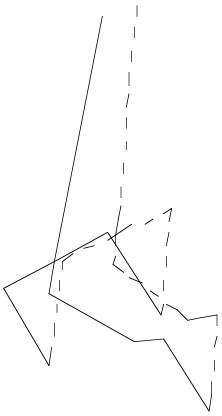

(b) Balance-frame lateral mode at 2.46 Hz.

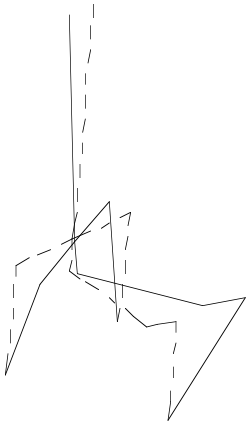

(e) Test-stand yaw mode at 6.78 Hz.

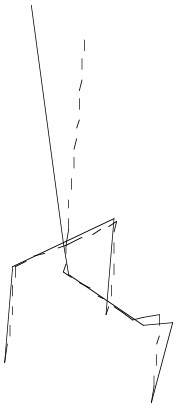

(c) Test-stand 1st longitudinal mode at 2.80 Hz.

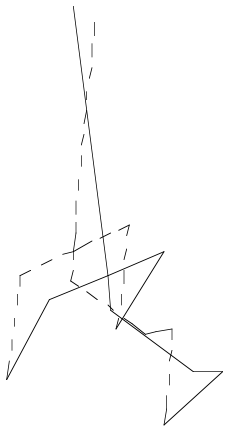

(f) Test-stand 2nd longitudinal mode at 7.23 Hz.

Figure 7. Modal display for the dampers-off configuration.

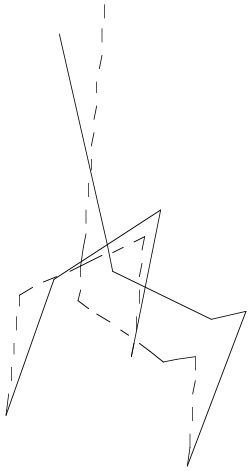

(g) Test-stand 2nd lateral mode at 9.20 Hz.

Figure 7. Concluded.

Appendix A

Frequency Response Plots of Accelerometers and Rotor Balance

Frequency Response Plots

Appendix A includes the frequency response plots of accelerometers and rotor-balance for three test configurations (dampers-off, dampers-on, and locked). Figures A-1–A-3 show the responses out to 16 Hz for all accelerometers. Figures A-4–A-6 show the responses out to 64 Hz for the hub accelerometers. The nodal location, the response direction, and the excitation direction are presented in the parenthesis, e.g. (1X+, 1X–) for hub longitudinal response caused by longitudinal excitation. Finally, figures A-7 to A-9 show the rotor-balance responses out to 64 Hz.

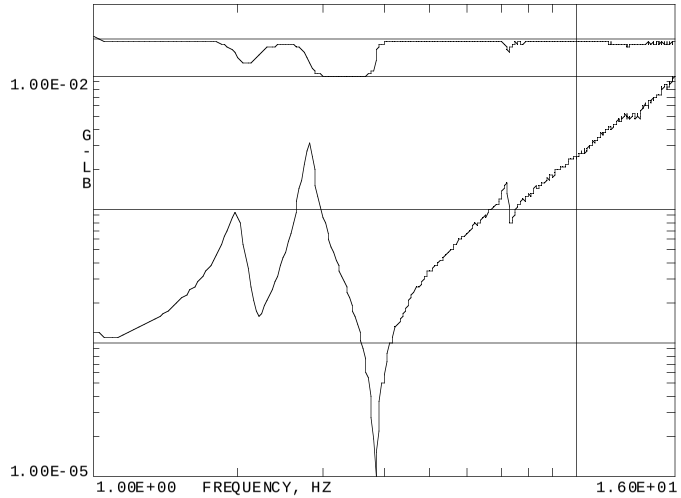

(a) Hub longitudinal response to longitudinal excitation. (1X+, 1X–)

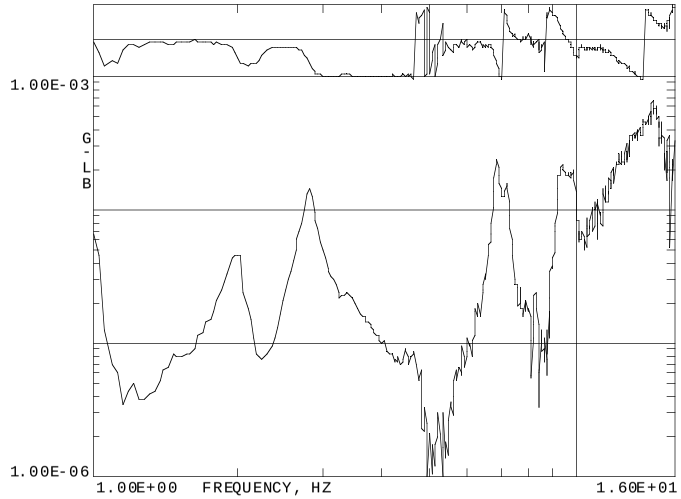

(b) Hub lateral response to longitudinal excitation. (1Y+, 1X–)

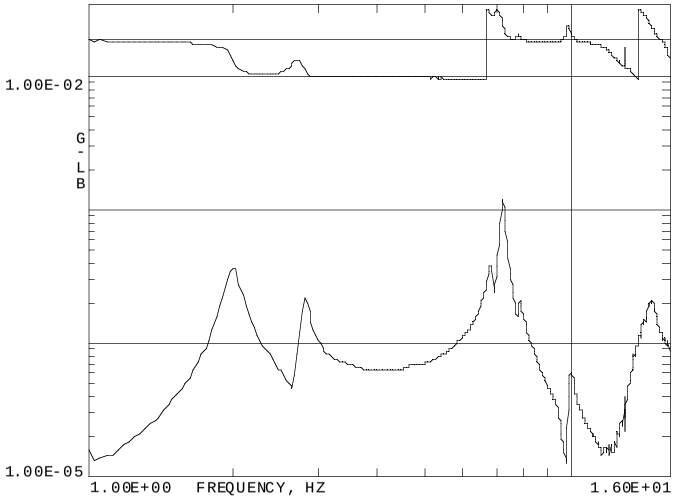

(c) Left strut longitudinal response to longitudinal excitation. (3X+, 1X–)

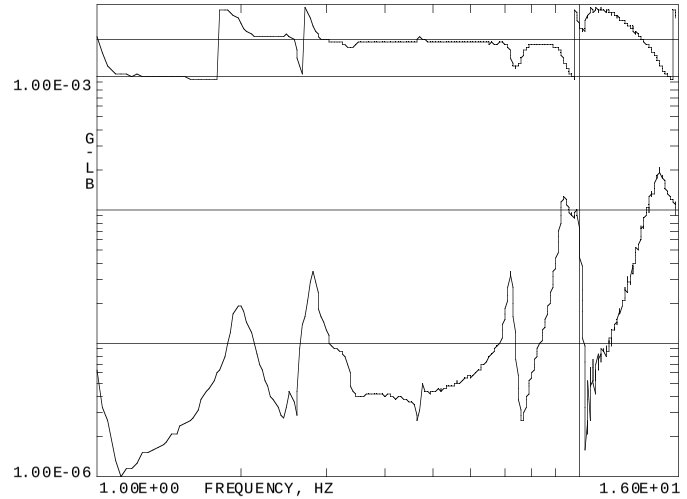

(d) Left strut lateral response to longitudinal excitation. (3Y+, 1X–)

Figure A-1. Frequency response functions for the dampers-off configuration.

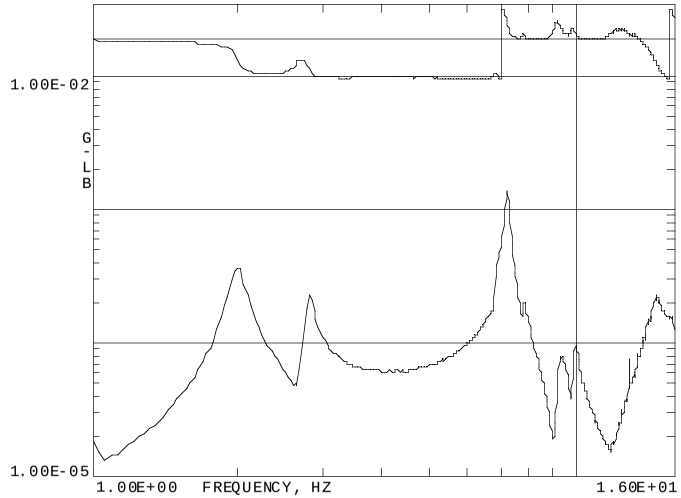

(e) Right strut longitudinal response to longitudinal excitation. (4X+, 1X–)

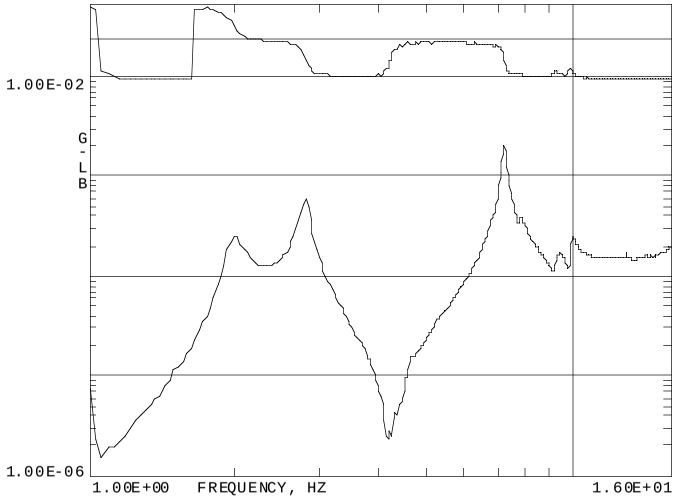

(g) Tail strut longitudinal response to longitudinal excitation. (8X–, 1X–)

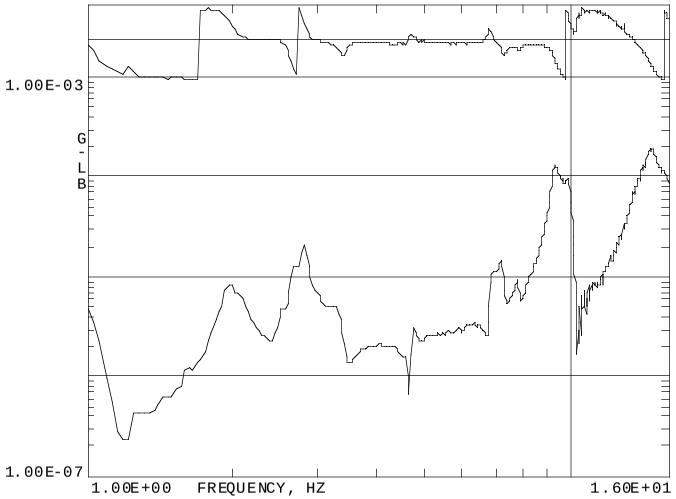

(f) Right strut lateral response to longitudinal excitation. (4Y+, 1X–)

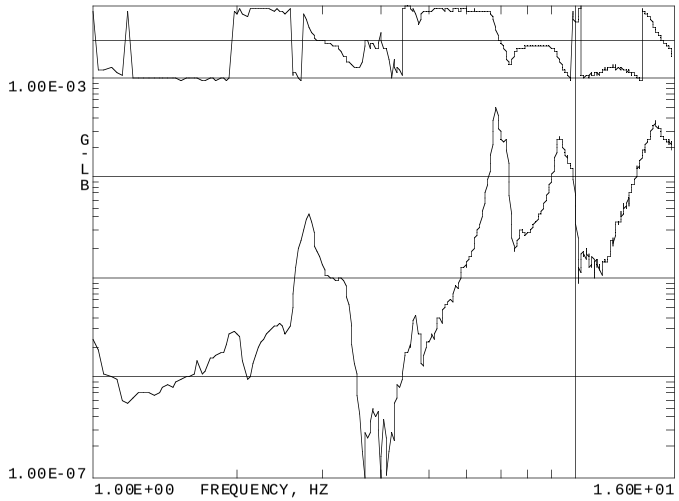

(h) Tail strut lateral response to longitudinal excitation. (8Y+, 1X–)

Figure A-1. Continued.

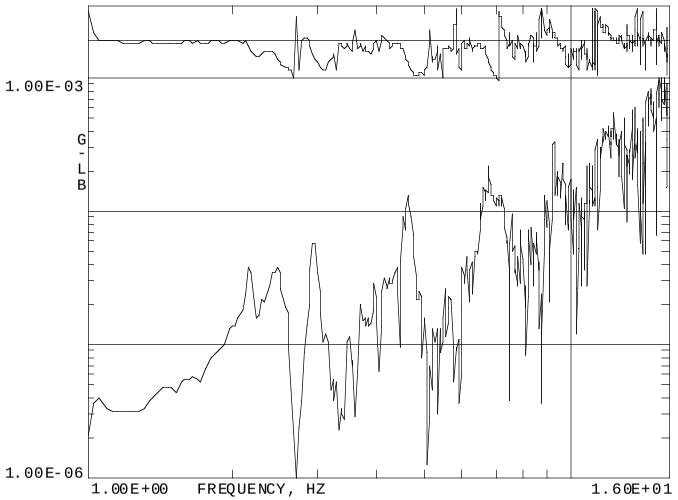

(i) Hub longitudinal response to lateral excitation. (1X+, 1Y–)

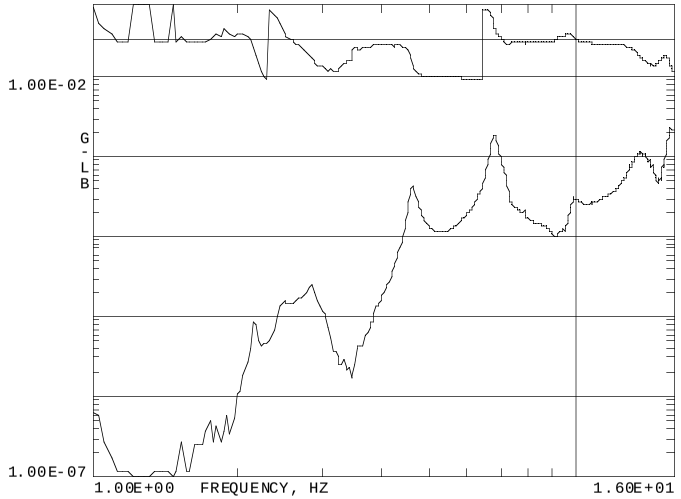

(k) Left strut longitudinal response to lateral excitation. (3X+, 1Y–)

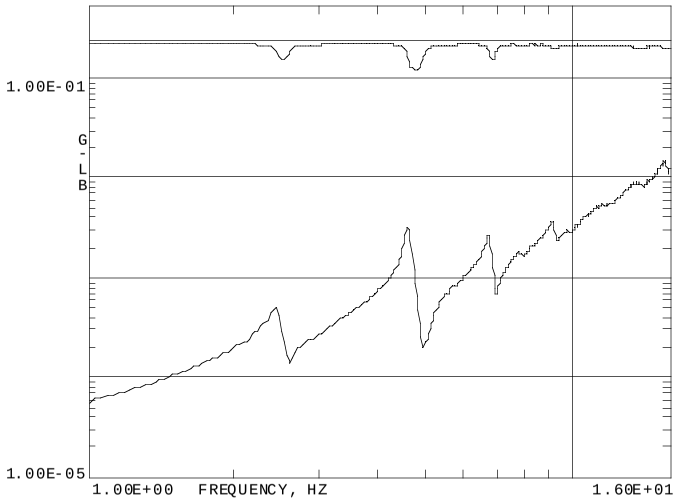

(j) Hub lateral response to lateral excitation. (1Y+, 1Y–).

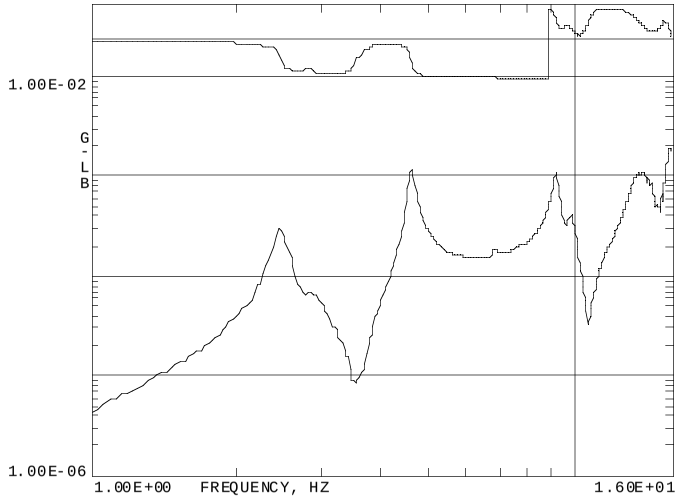

(l) Left strut lateral response to lateral excitation. (3Y+, 1Y–)

Figure A-1. Continued.

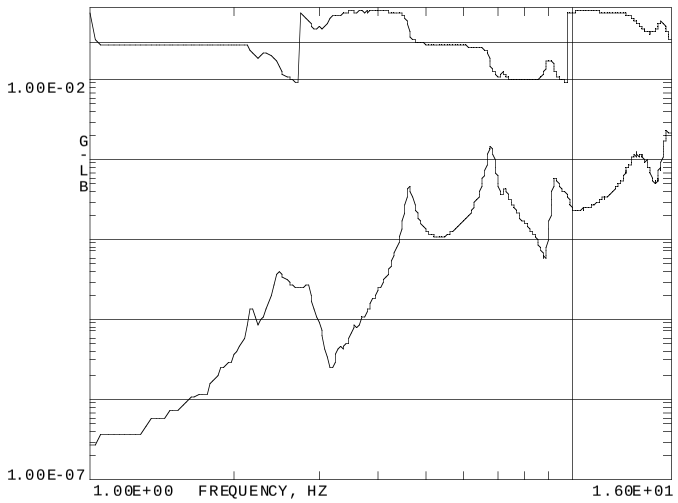

(m) Right strut longitudinal response to lateral excitation. (4X+, 1Y–)

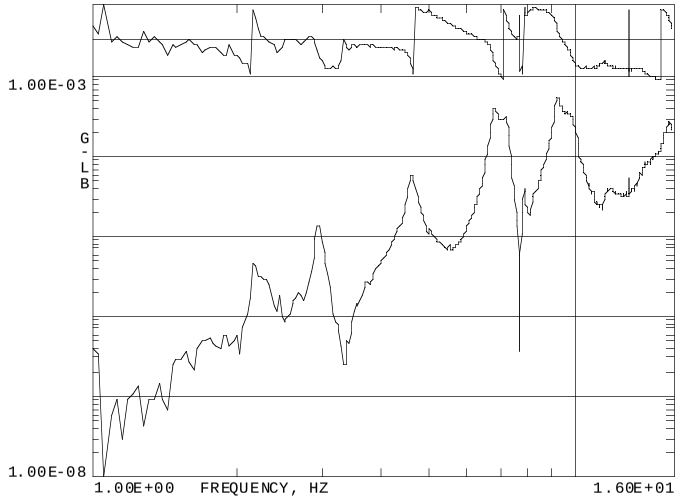

(o) Tail strut longitudinal response to lateral excitation. (8X–, 1Y–)

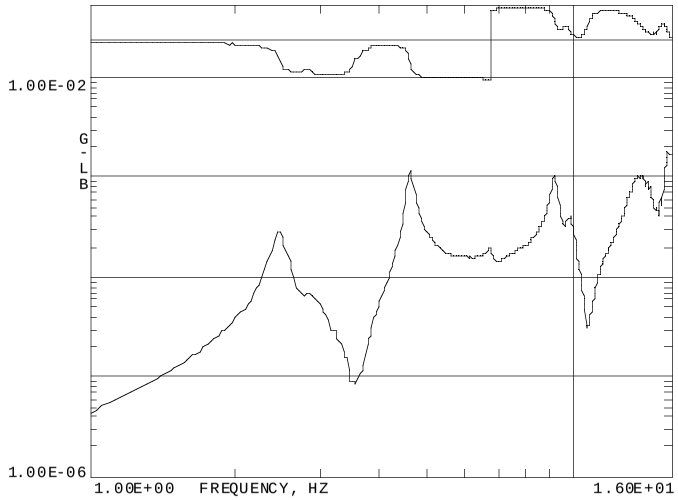

(n) Right strut lateral response to lateral excitation. (4Y+, 1Y–)

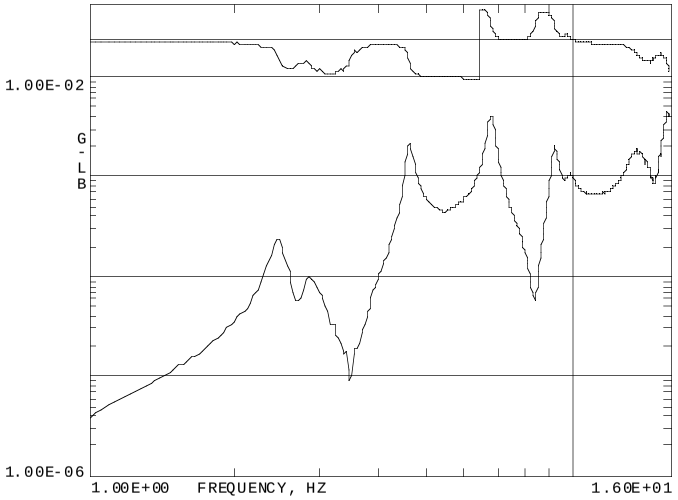

(p) Tail strut lateral response to lateral excitation. (8Y+, 1Y–)

Figure A-1. Concluded.

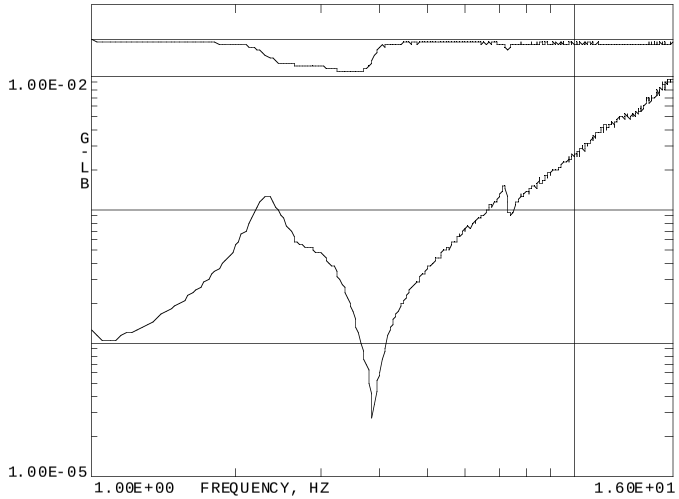

(a) Hub longitudinal response to longitudinal excitation. (1X+, 1X–)

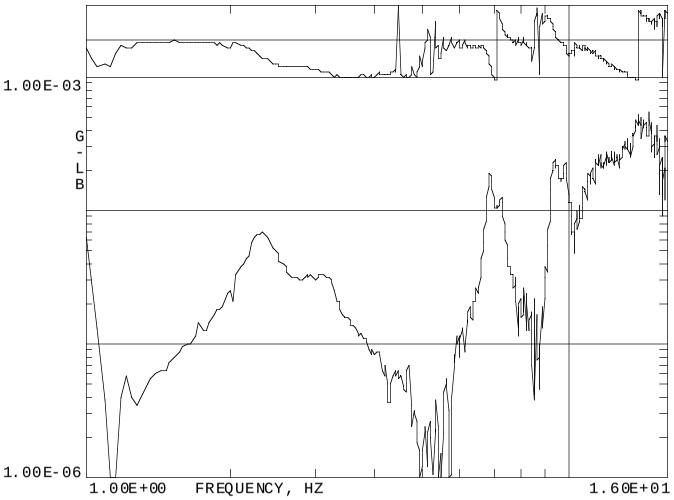

(b) Hub lateral response to longitudinal excitation. (1Y+, 1X–)

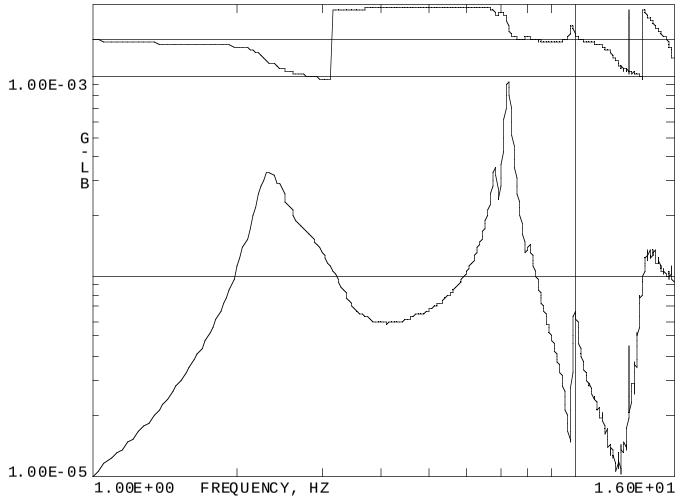

(c) Left strut longitudinal response to longitudinal excitation. (3X+, 1X–)

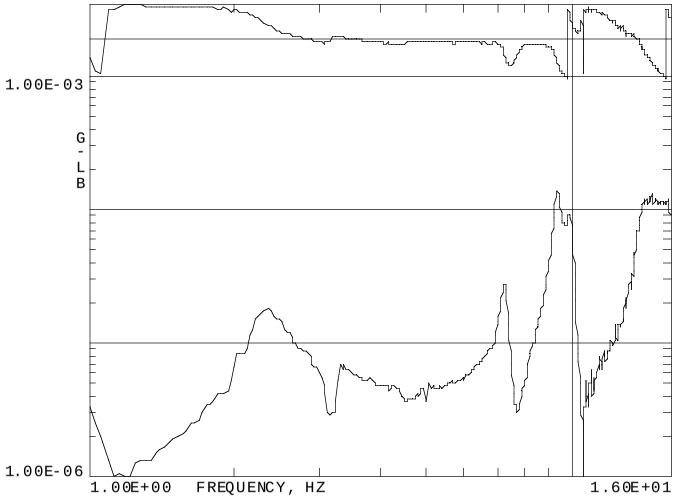

(d) Left strut lateral response to longitudinal excitation. (3Y+, 1X–)

Figure A-2. Frequency response functions for the dampers-on configuration.

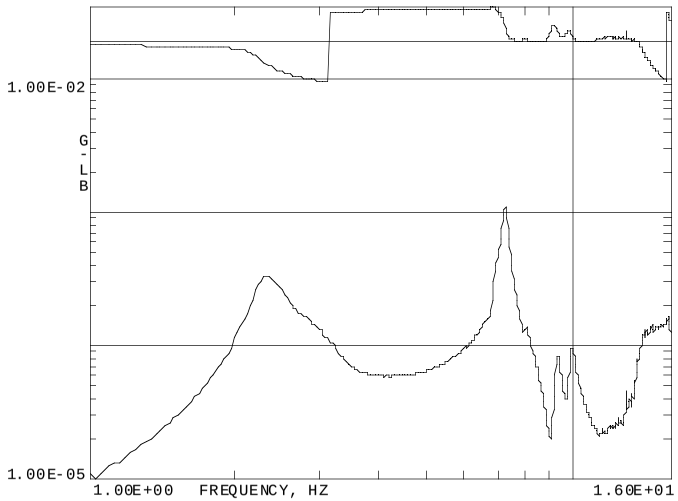

(e) Right strut longitudinal response to longitudinal excitation. (4X+, 1X–)

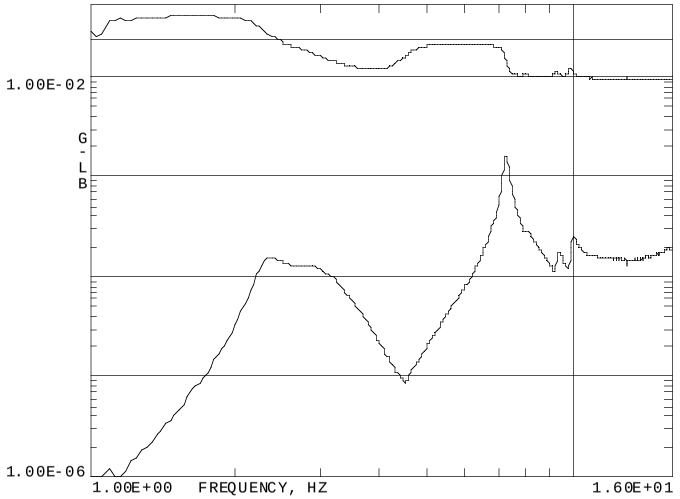

(g) Tail strut longitudinal response to longitudinal excitation. (8X–, 1X–)

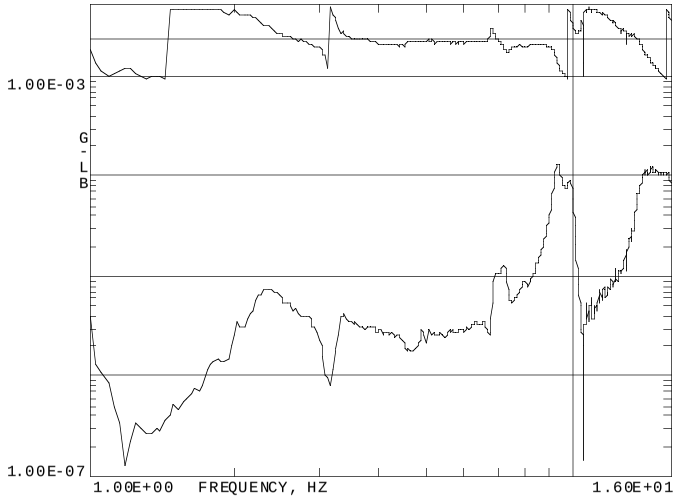

(f) Right strut lateral response to longitudinal excitation. (4Y+, 1X–)

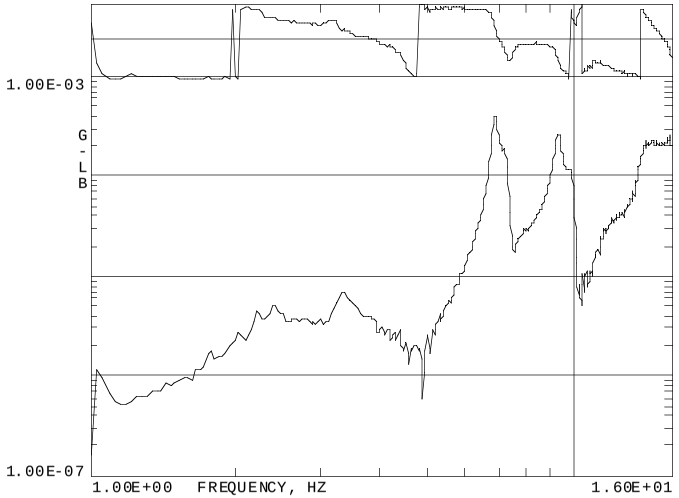

(h) Tail strut lateral response to longitudinal excitation. (8Y+, 1X–)

Figure A-2. Continued.

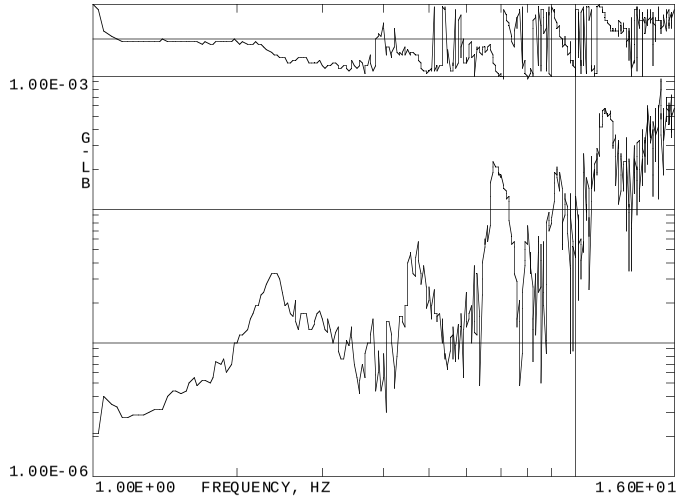

(i) Hub longitudinal response to lateral excitation. (1X+, 1Y–)

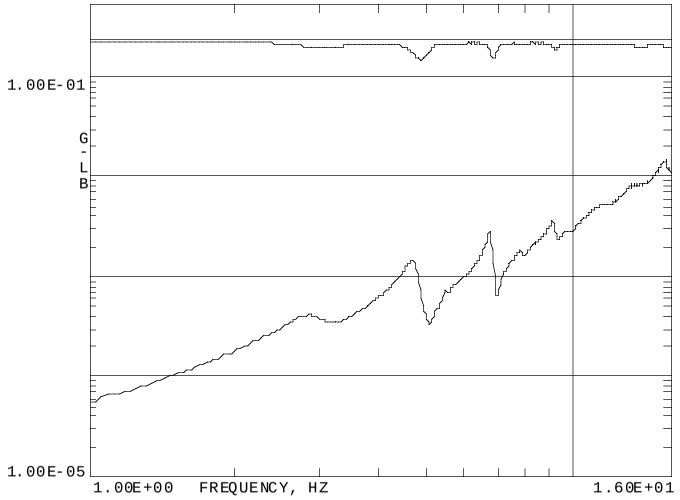

(j) Hub lateral response to lateral excitation. (1Y+, 1Y–)

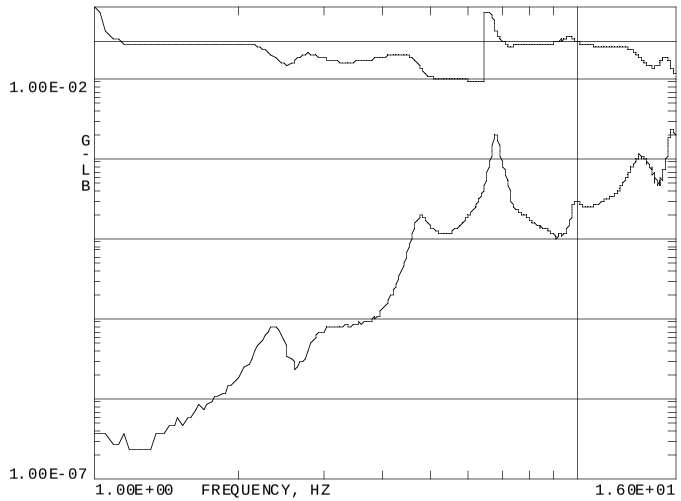

(k) Left strut longitudinal response to lateral excitation. (3X+, 1Y–)

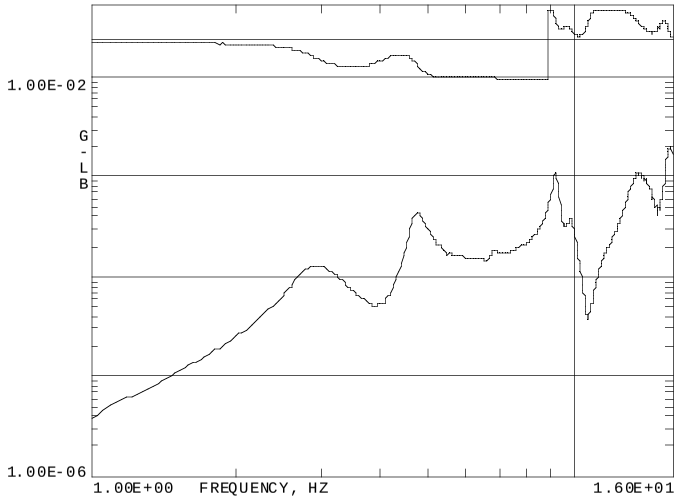

(l) Left strut lateral response to lateral excitation. (3Y+, 1Y–)

Figure A-2. Continued.

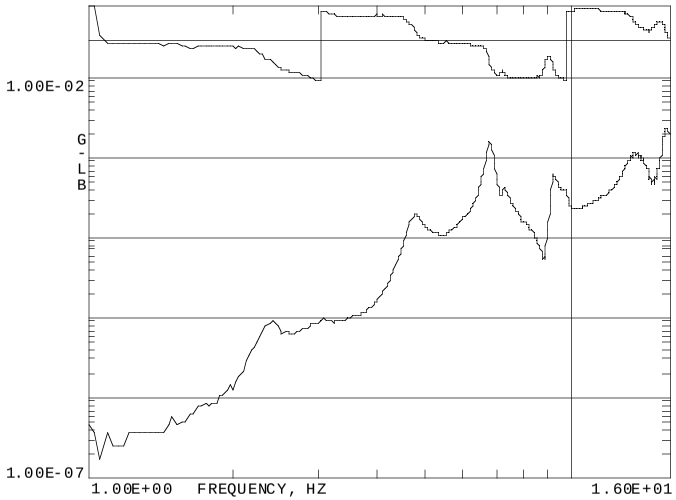

(m) Right strut longitudinal response to lateral excitation. (4X+, 1Y–)

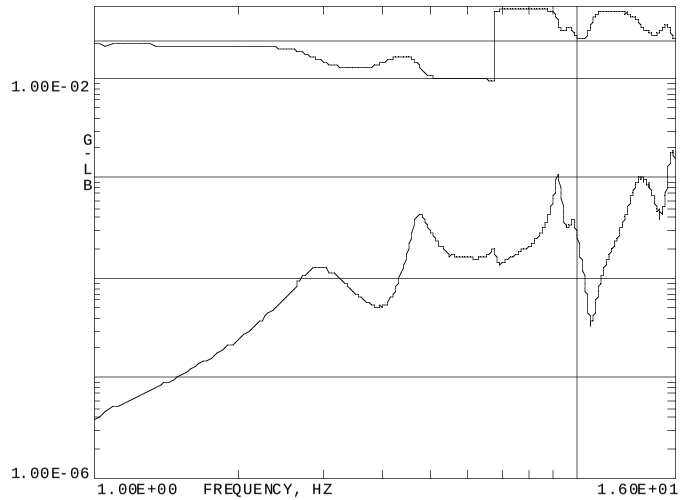

(n) Right strut lateral response to lateral excitation. (4Y+, 1Y–)

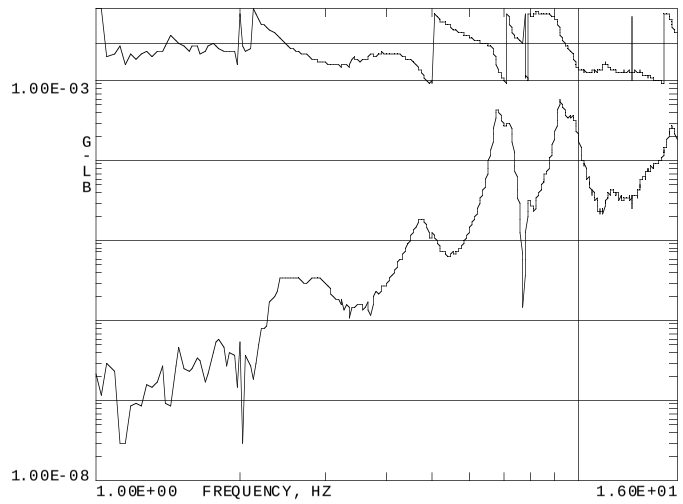

(o) Tail strut longitudinal response to lateral excitation. (8X–, 1Y–)

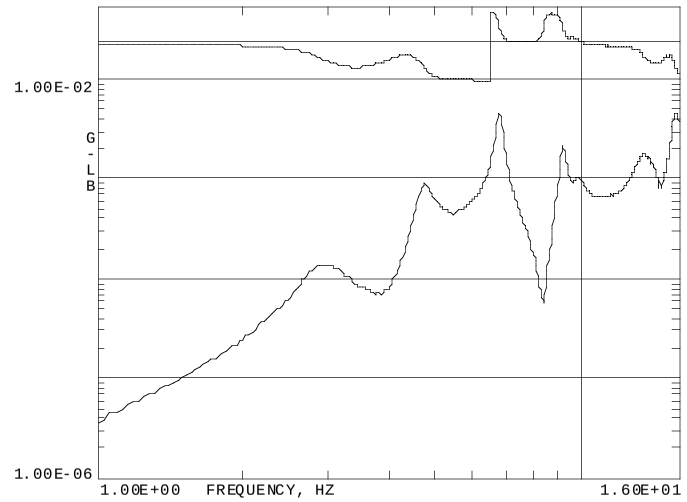

(p) Tail strut lateral response to lateral excitation. (8Y+, 1Y–)

Figure A-2. Concluded.

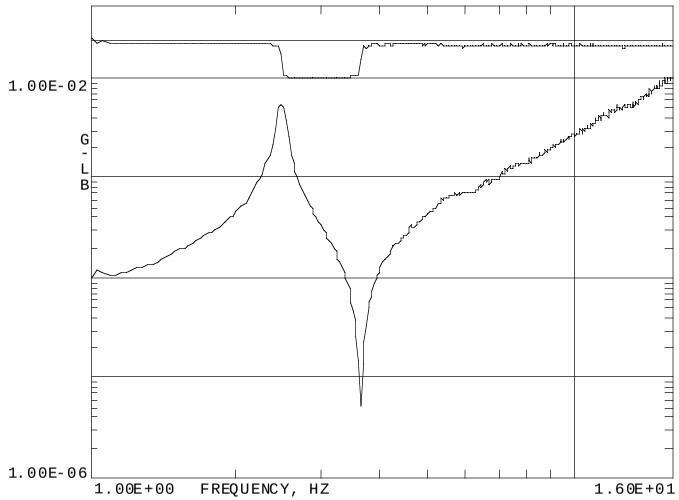

(a) Hub longitudinal response to longitudinal excitation. (1X+, 1X–)

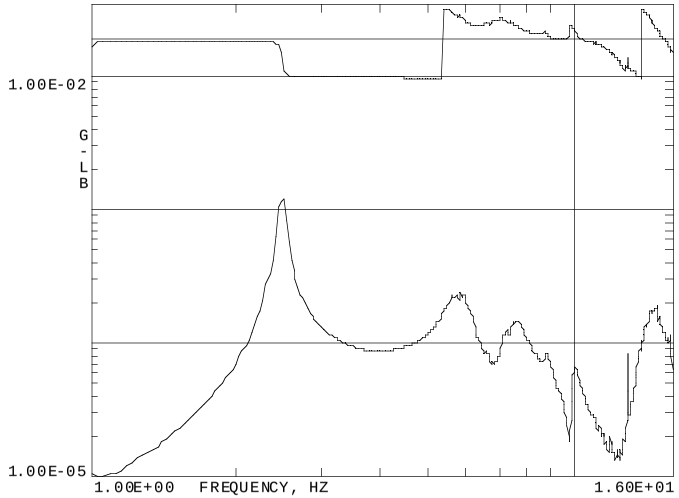

(c) Left strut longitudinal response to longitudinal excitation. (3X+, 1X–)

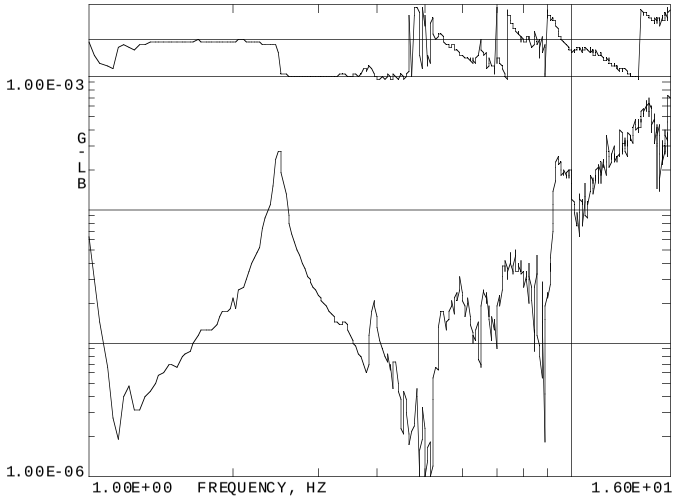

(b) Hub lateral response to longitudinal excitation. (1Y+, 1X–)

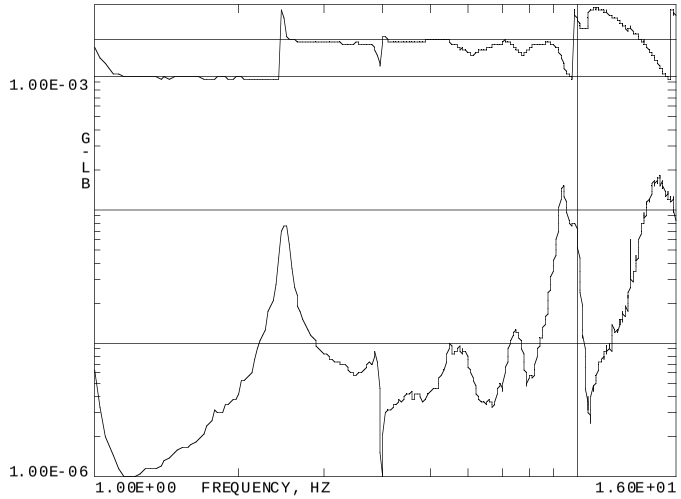

(d) Left strut lateral response to longitudinal excitation. (3Y+, 1X–)

Figure A-3. Frequency response functions for the locked configuration.

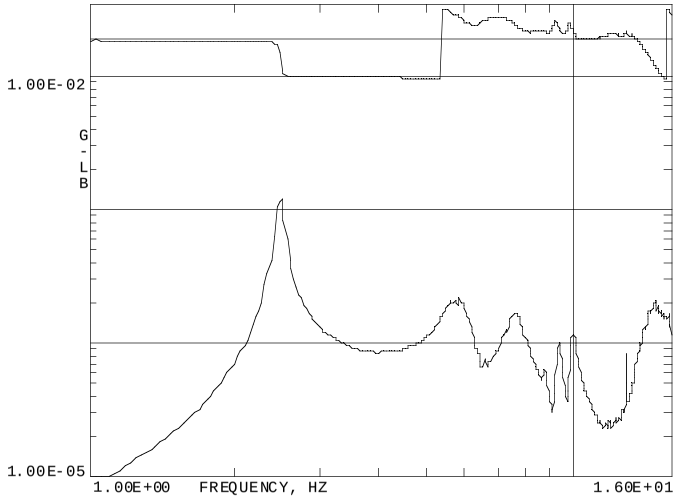

(e) Right strut longitudinal response to longitudinal excitation. (4X+, 1X–)

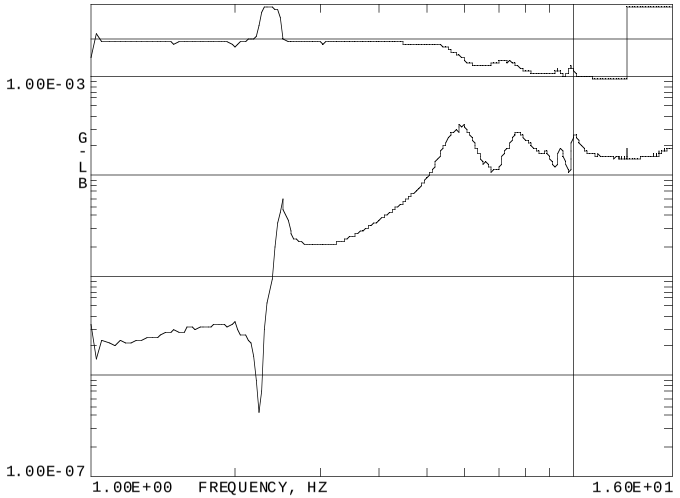

(g) Tail strut longitudinal response to longitudinal excitation. (8X–, 1X–)

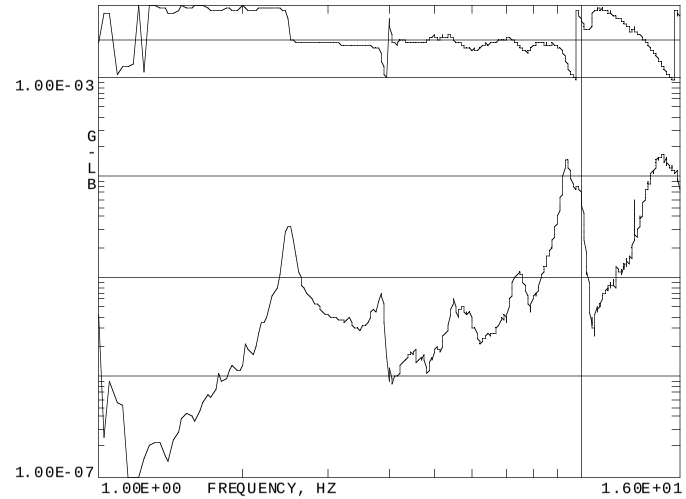

(f) Right strut lateral response to longitudinal excitation. (4Y+, 1X–)

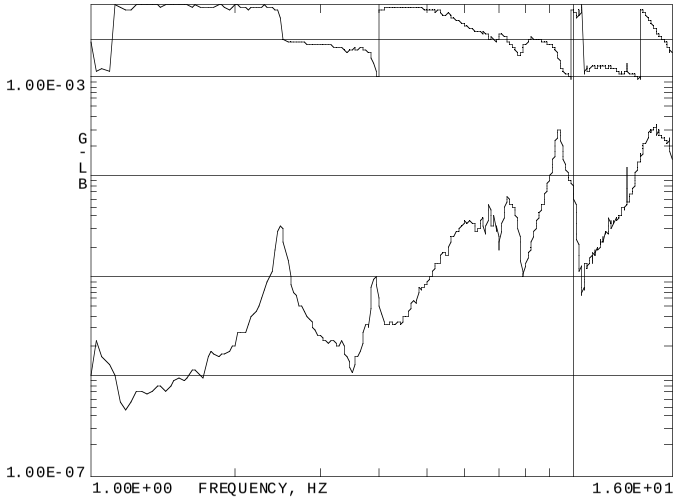

(h) Tail strut lateral response to longitudinal excitation. (8Y+, 1X–).

Figure A-3. Continued.

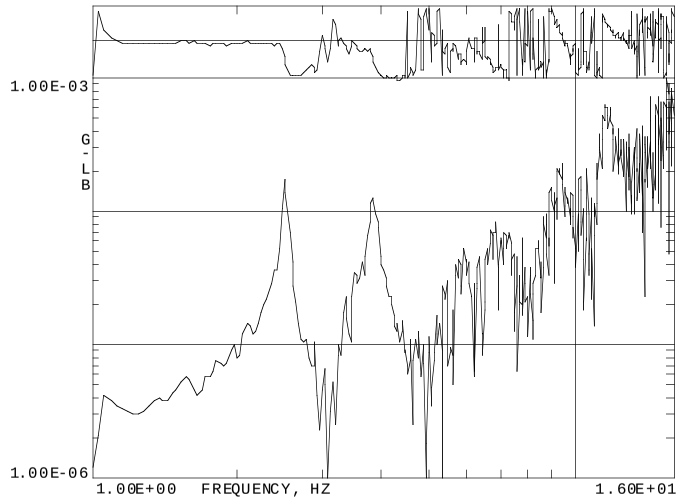

(i) Hub longitudinal response to lateral excitation. (1X+, 1Y–)

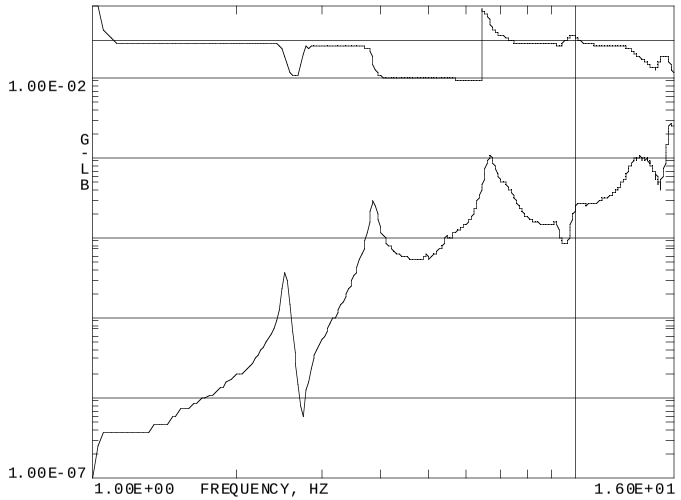

(k) Left strut longitudinal response to lateral excitation. (3X+, 1Y–)

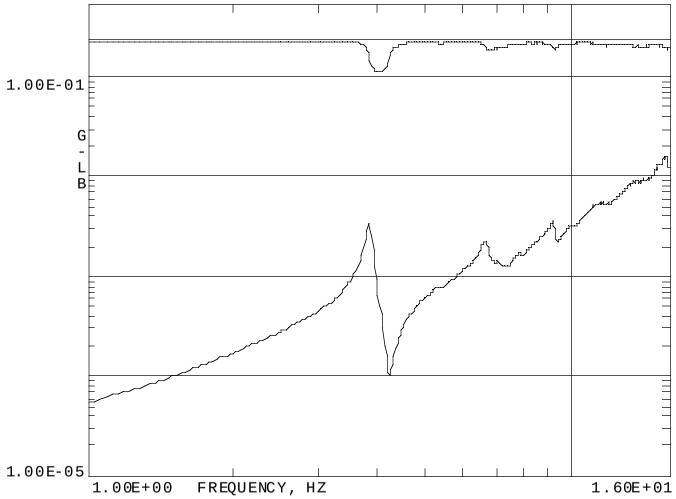

(j) Hub lateral response to lateral excitation. (1Y+, 1Y–)

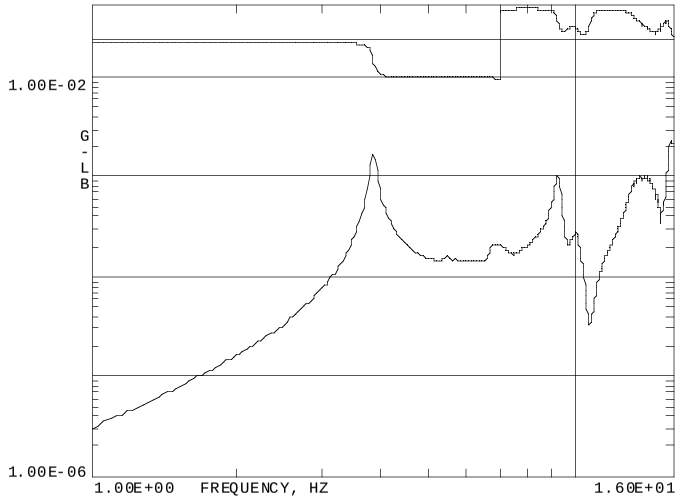

(l) Left strut lateral response to lateral excitation. (3Y+, 1Y–)

Figure A-3. Continued.

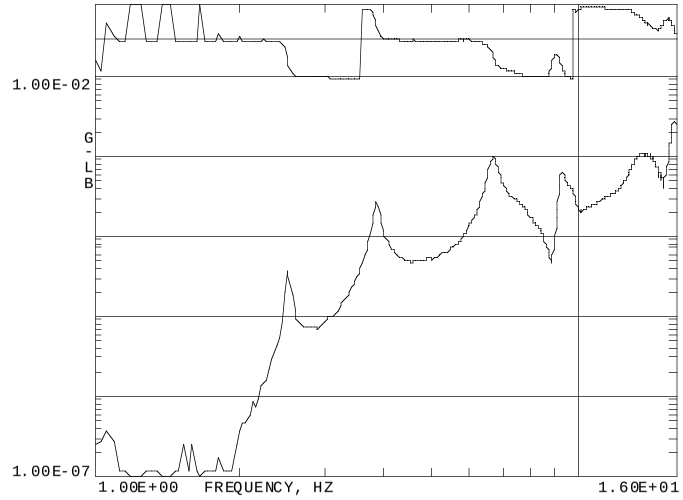

(m) Right strut longitudinal response to lateral excitation. (4X+, 1Y–)

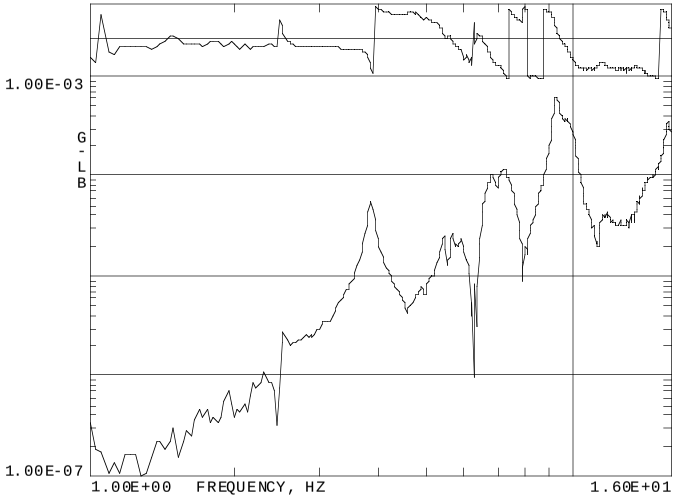

(o) Tail strut longitudinal response to lateral excitation. (8X–, 1Y–)

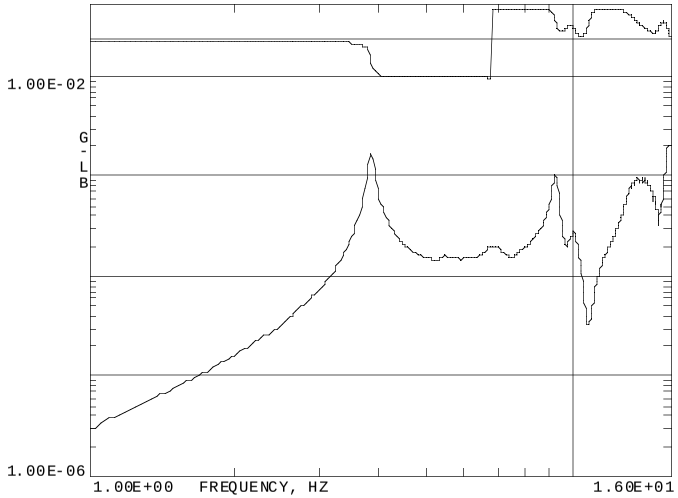

(n) Right strut lateral response to lateral excitation. (4Y+, 1Y–)

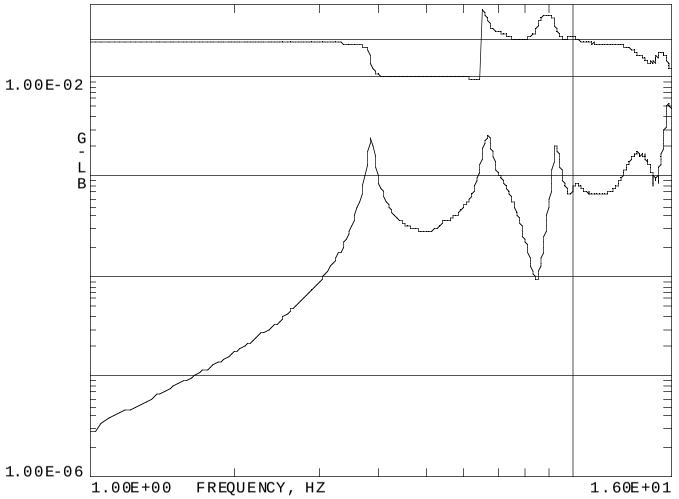

(p) Tail strut lateral response to lateral excitation. (8Y+, 1Y–)

Figure A-3. Concluded.

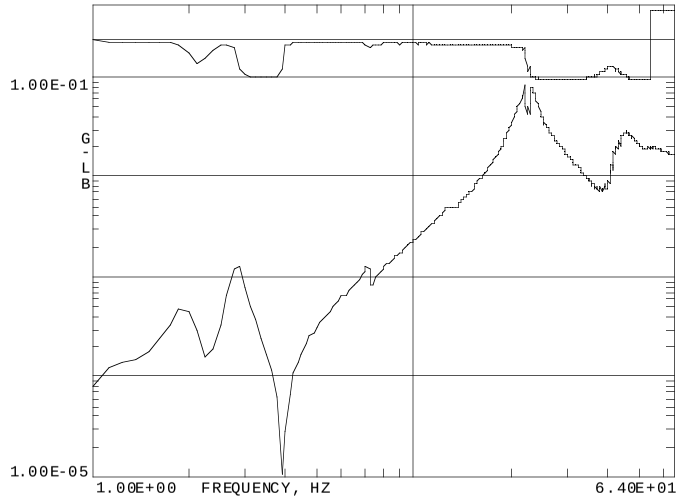

(a) Hub longitudinal response to longitudinal excitation. (1X+, 1X–)

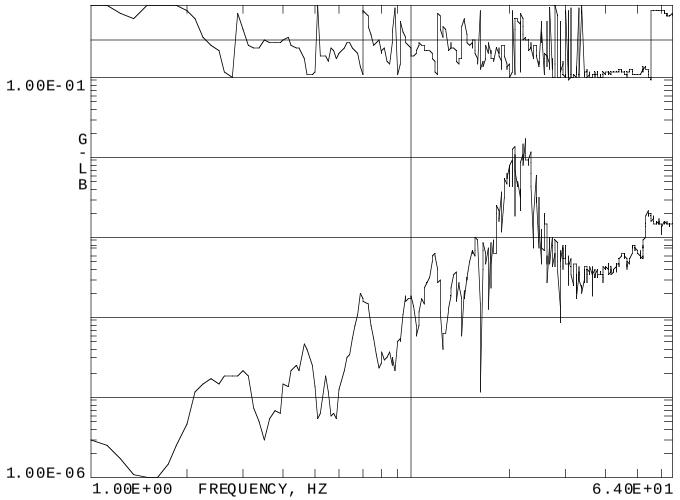

(c) Hub longitudinal response to lateral excitation. (1X+, 1Y–)

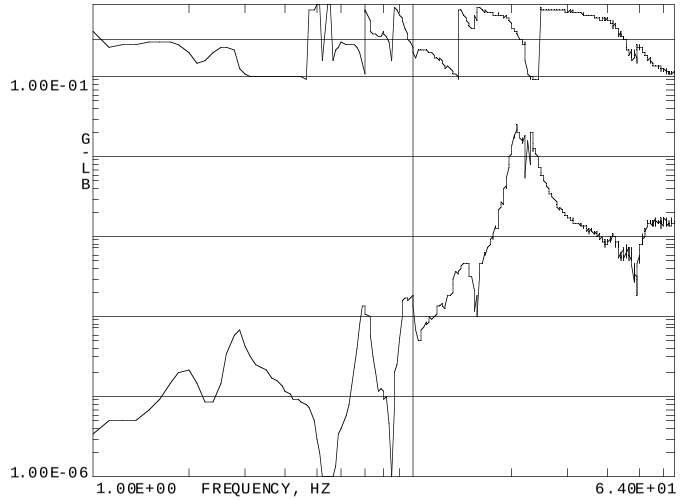

(b) Hub lateral response to longitudinal excitation. (1Y+, 1X–)

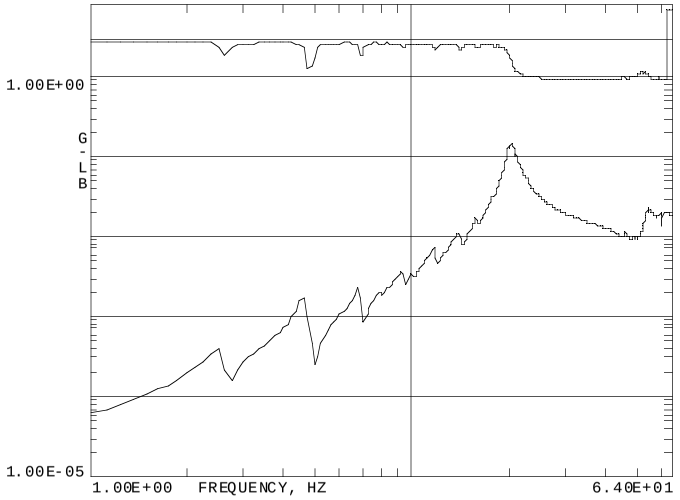

(d) Hub lateral response to lateral excitation. (1Y+, 1Y–)

Figure A-4. Frequency response functions of the rotor hub for the dampers-off configuration.

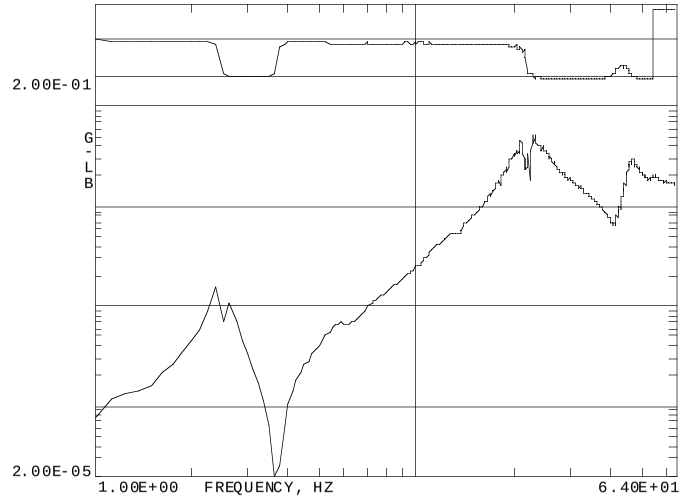

(a) Hub longitudinal response to longitudinal excitation. (1X+, 1X–)

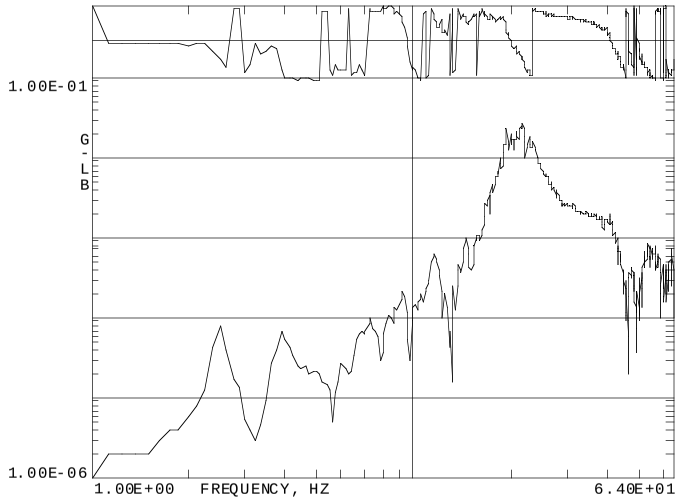

(c) Hub longitudinal response to lateral excitation. (1X+, 1Y–)

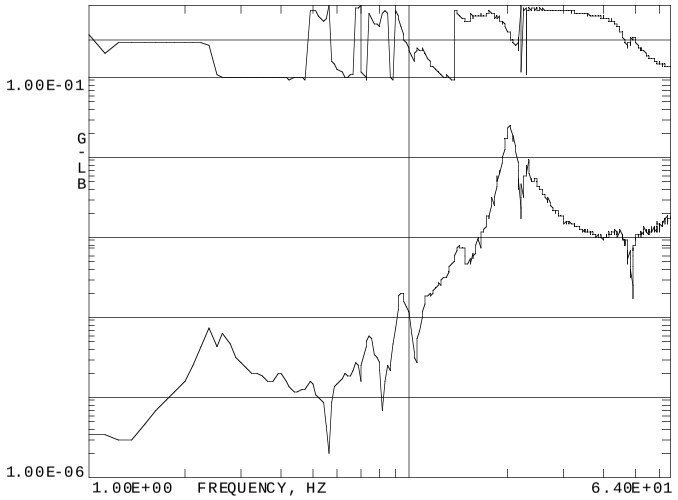

(b) Hub lateral response to longitudinal excitation. (1Y+, 1X–)

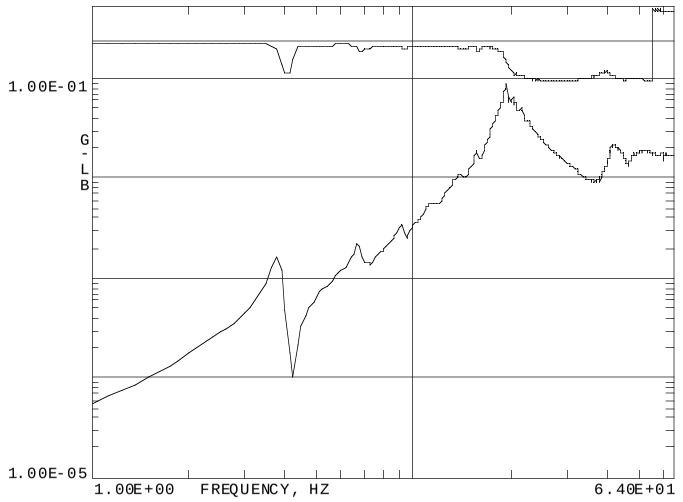

(d) Hub lateral response to lateral excitation. (1Y+, 1Y–)

Figure A-5. Frequency response functions of the rotor hub for the dampers-on configuration.

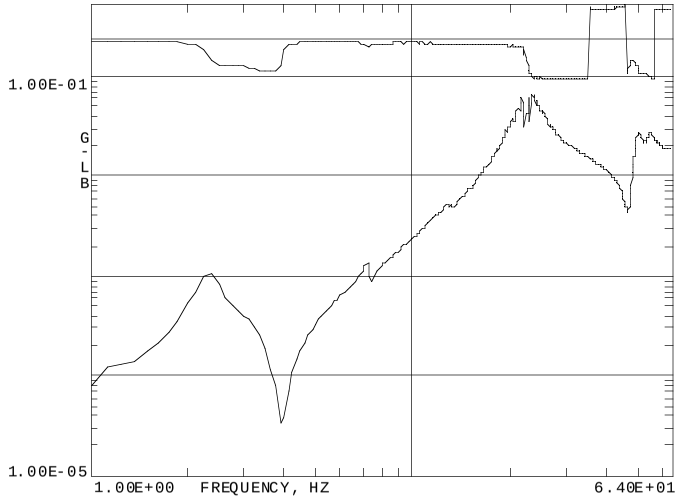

(a) Hub longitudinal response to longitudinal excitation. (1X+, 1X–)

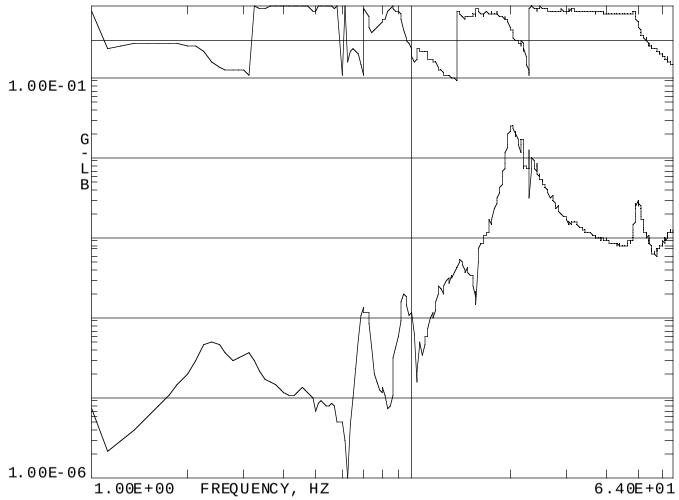

(b) Hub lateral response to longitudinal excitation. (1Y+, 1X–)

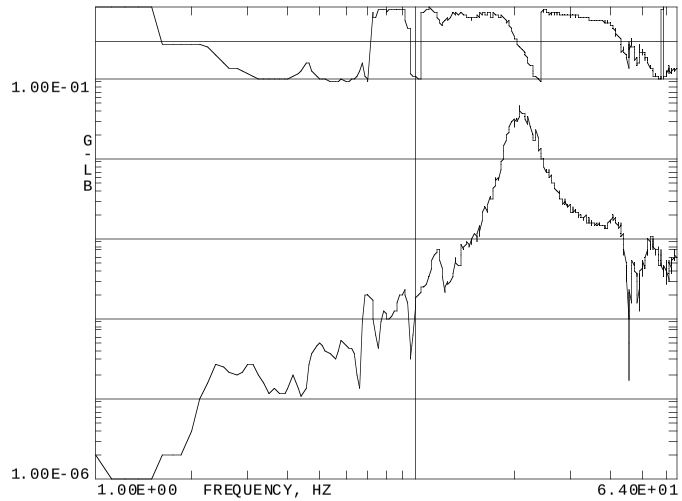

(c) Hub longitudinal response to lateral excitation. (1X+, 1Y–)

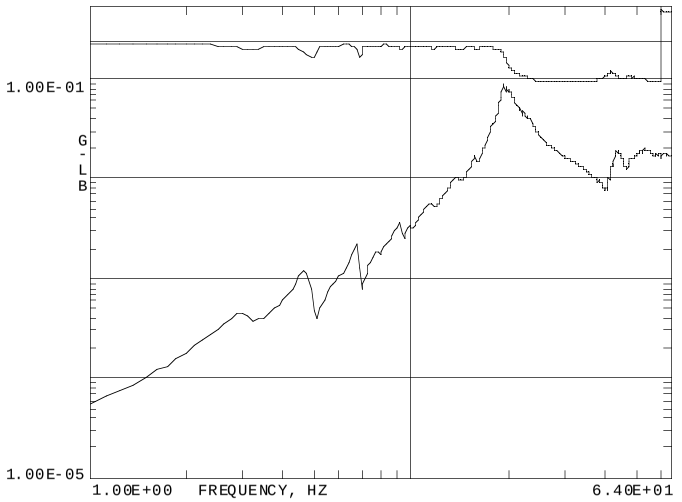

(d) Hub lateral response to lateral excitation. (1Y+, 1Y–)

Figure A-6. Frequency response functions of the rotor hub for the locked configuration

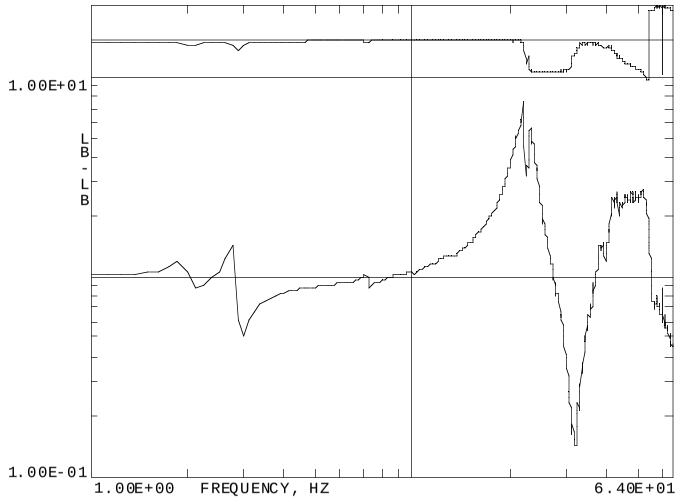

(a) Axial force response to longitudinal excitation.

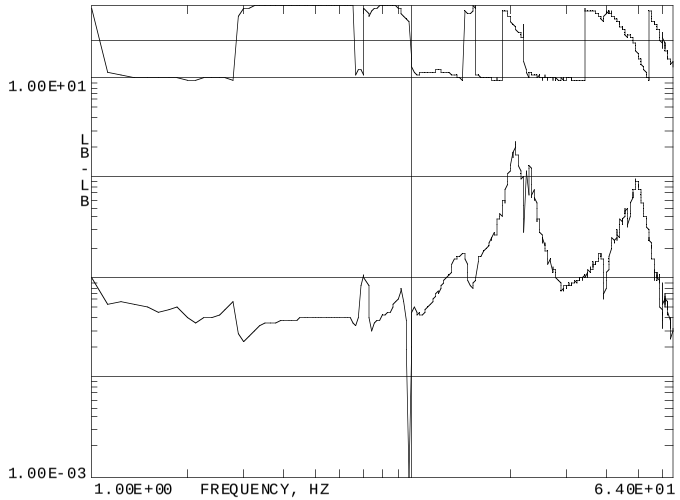

(b) Side force response to longitudinal excitation.

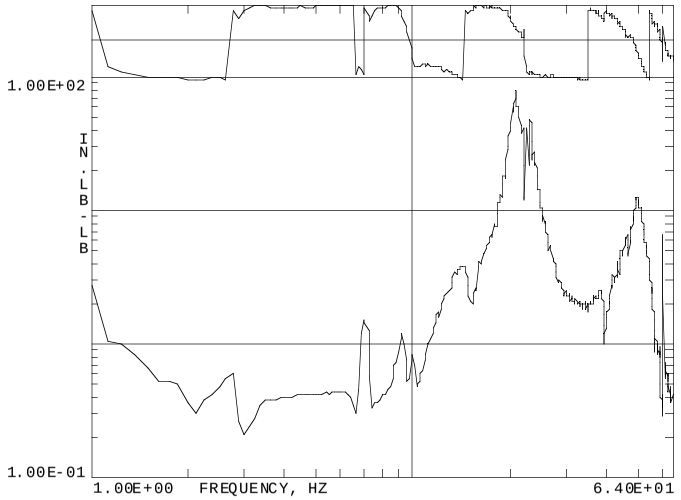

(c) Rolling moment response to longitudinal excitation.

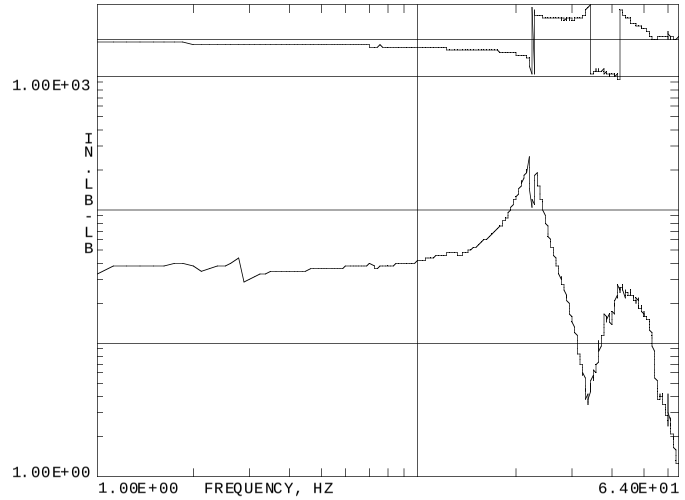

(d) Pitching moment response to longitudinal excitation.

Figure A-7. Frequency response functions of the rotor balance for the dampers-off configuration.

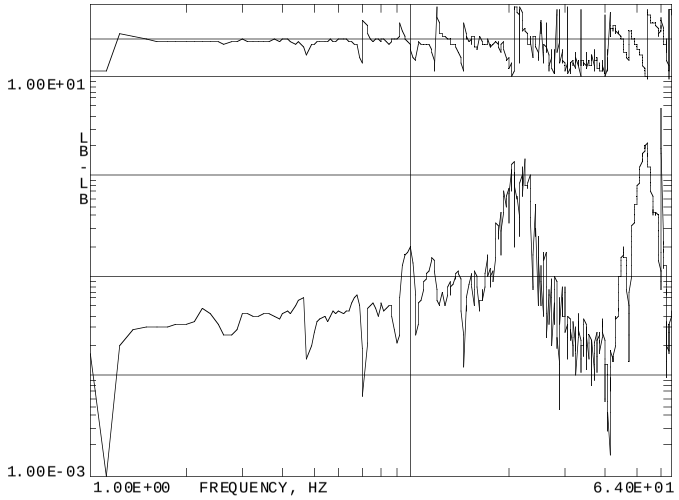

(e) Axial force response to lateral excitation.

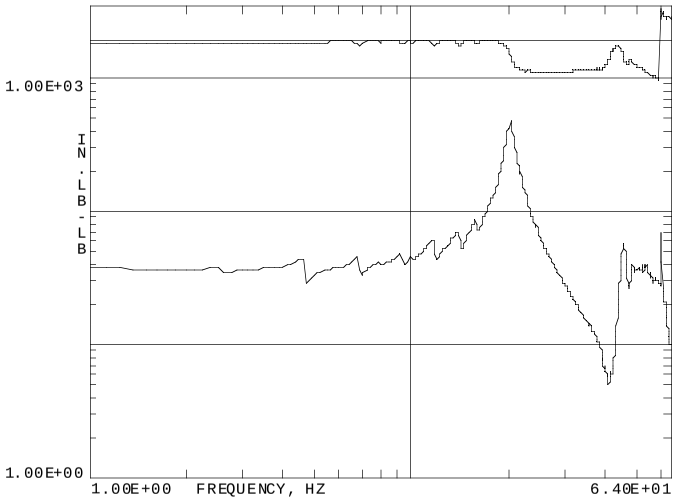

(g) Rolling moment response to lateral excitation.

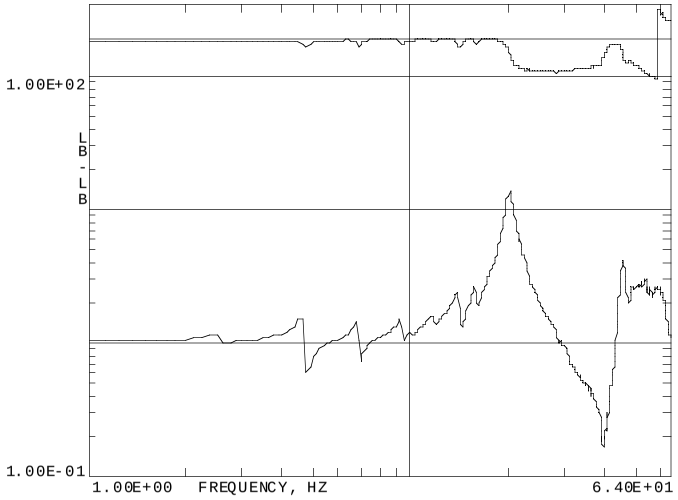

(f) Side force response to lateral excitation.

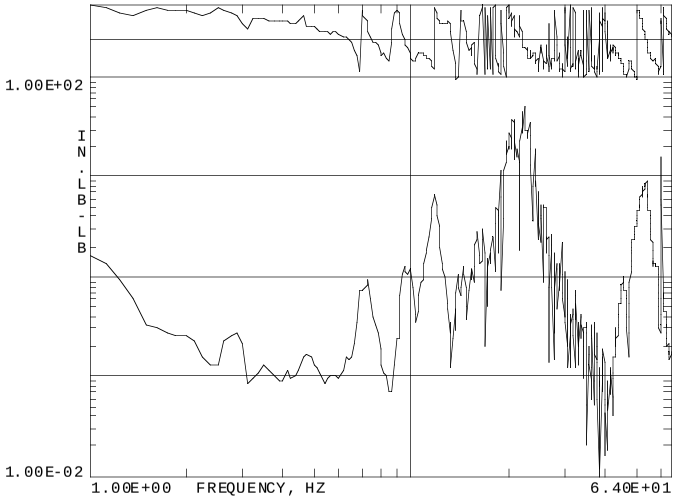

(h) Pitching moment response to lateral excitation.

Figure A-7. Concluded.

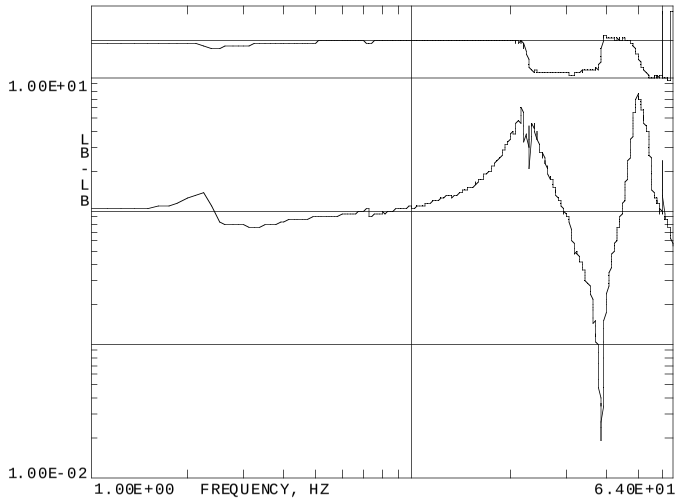

(a) Axial force response to longitudinal excitation.

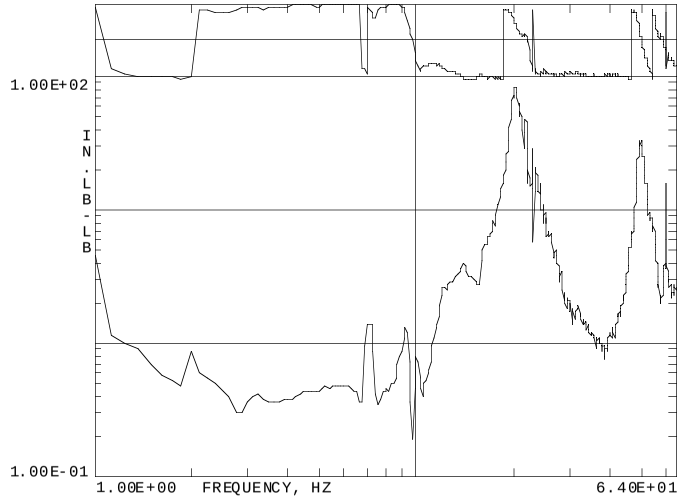

(c) Rolling moment response to longitudinal excitation.

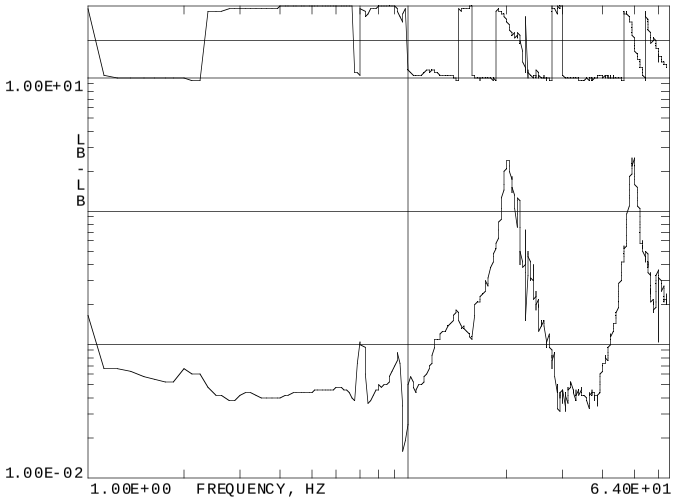

(b) Side force response to longitudinal excitation.

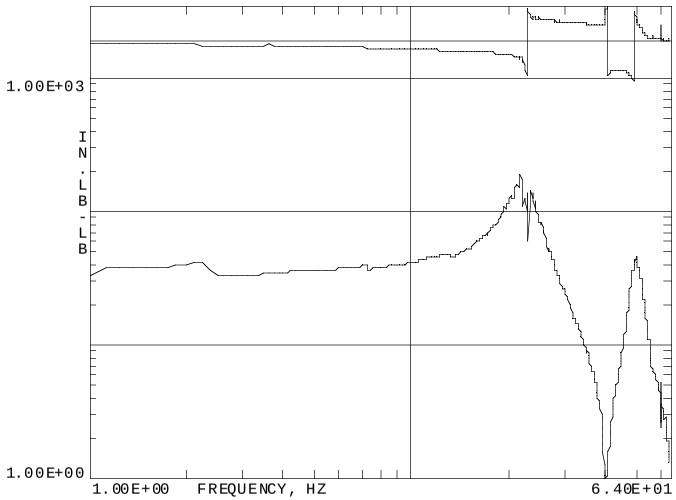

(d) Pitching moment response to longitudinal excitation.

Figure A-8. Frequency response functions of the rotor balance for the dampers-on configuration.

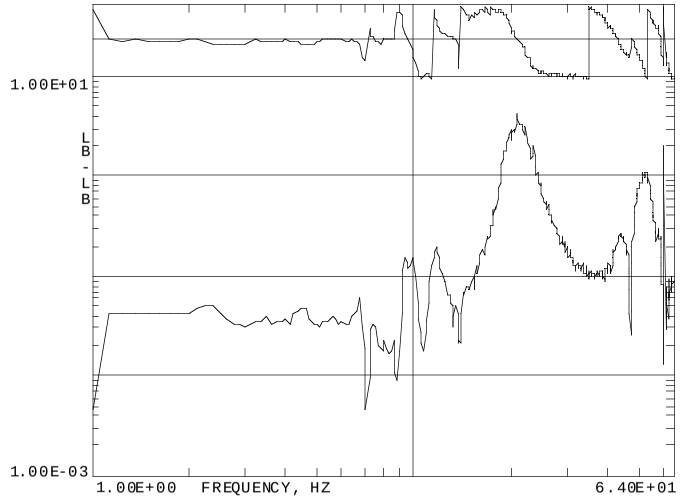

(e) Axial force response to lateral excitation.

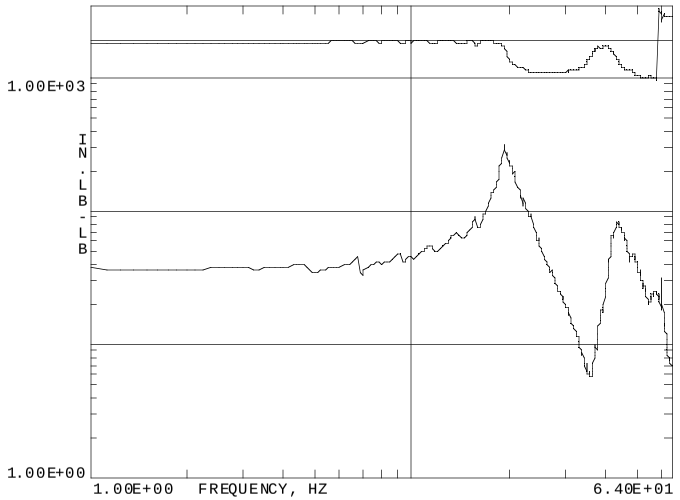

(g) Rolling moment response to lateral excitation.

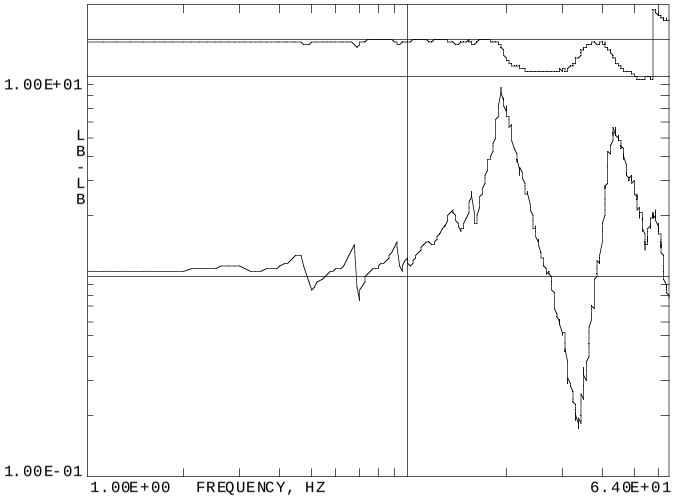

(f) Side force response to lateral excitation.

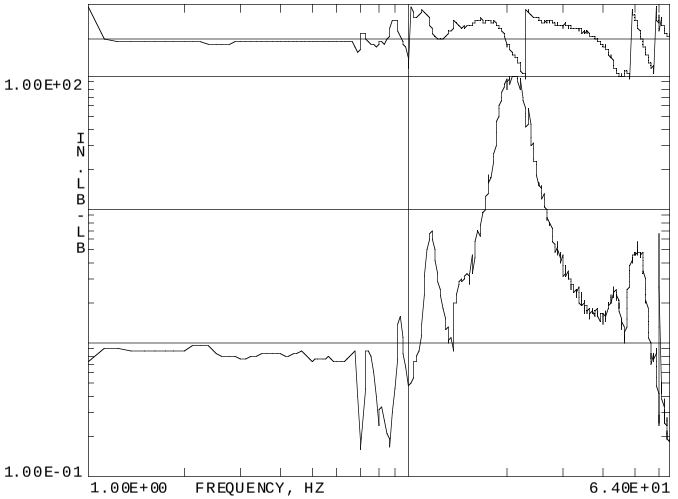

(h) Pitching moment response to lateral excitation

Figure A-8. Concluded.

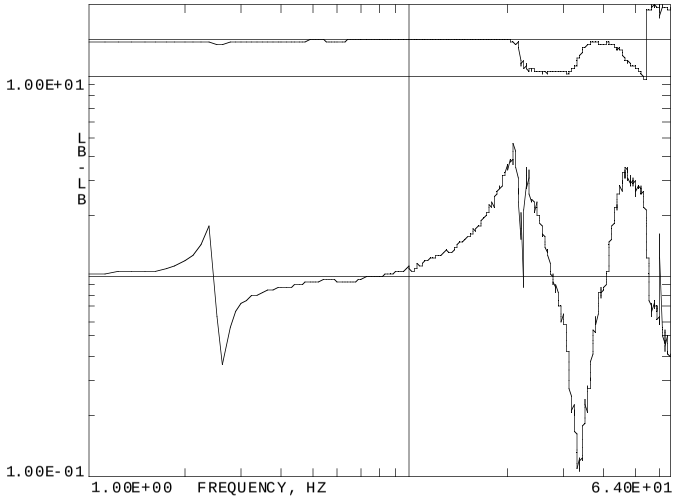

(a) Axial force response to longitudinal excitation.

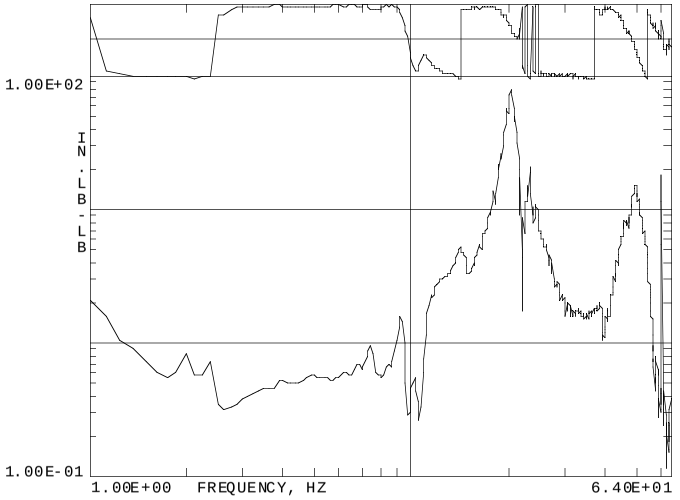

(c) Rolling moment response to longitudinal excitation.

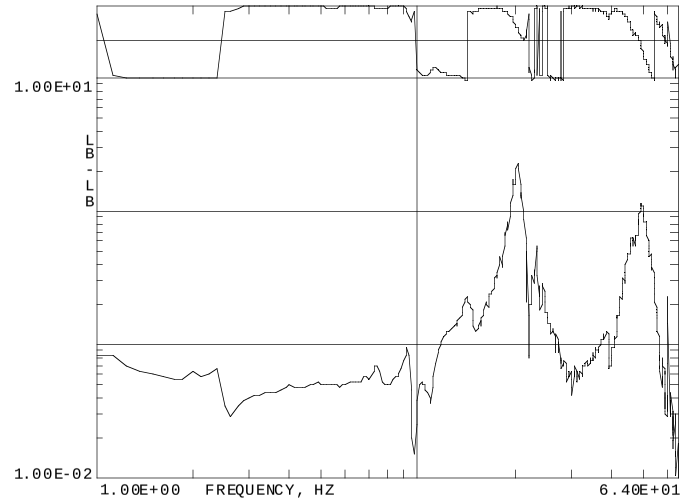

(b) Side force response to longitudinal excitation.

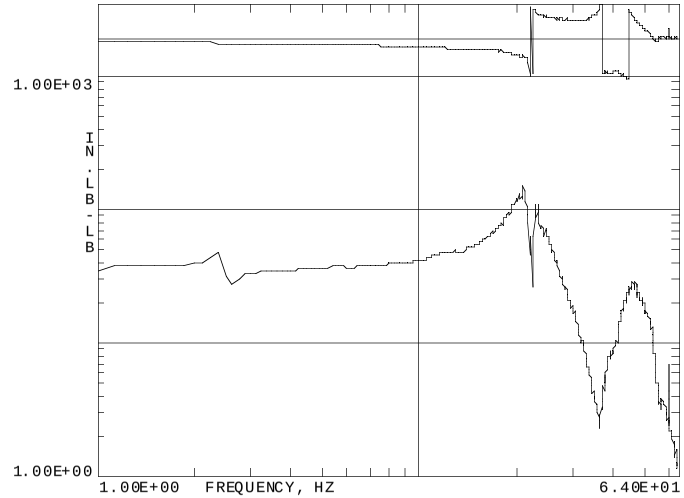

(d) Pitching moment response to longitudinal excitation.

Figure A-9. Frequency response functions of the rotor balance for the locked configuration.

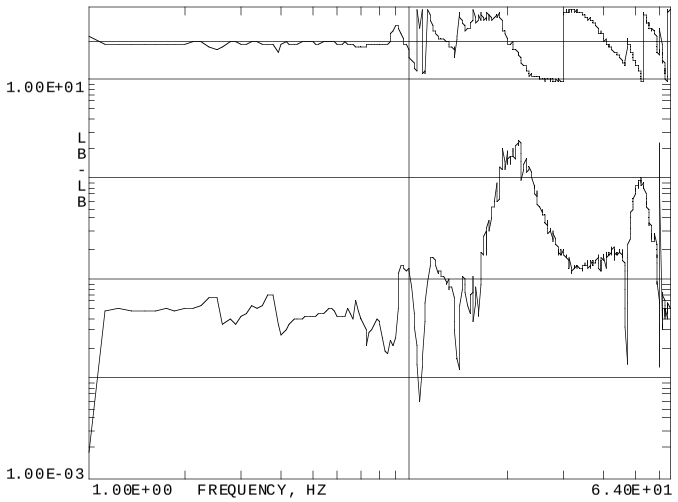

(e) Axial force response to lateral excitation.

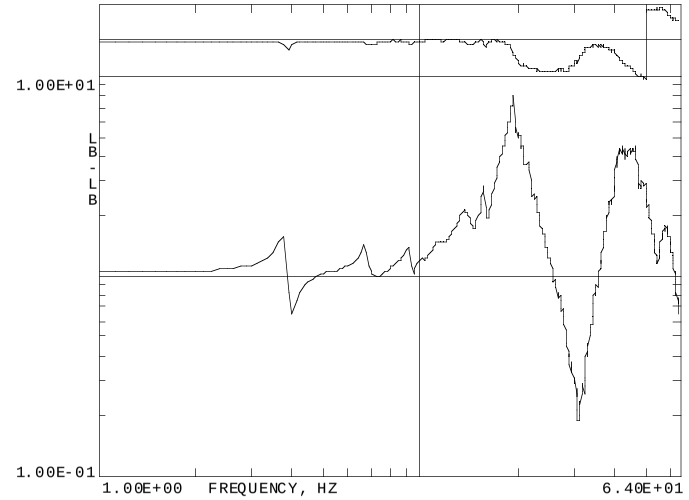

(f) Side force response to lateral excitation.

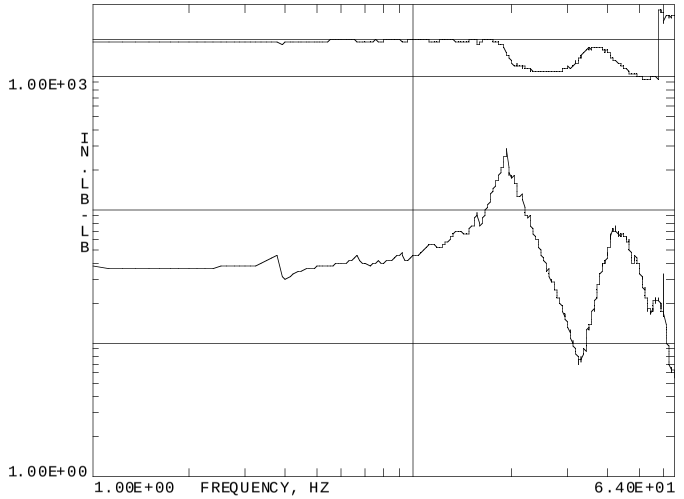

(g) Rolling moment response to lateral excitation.

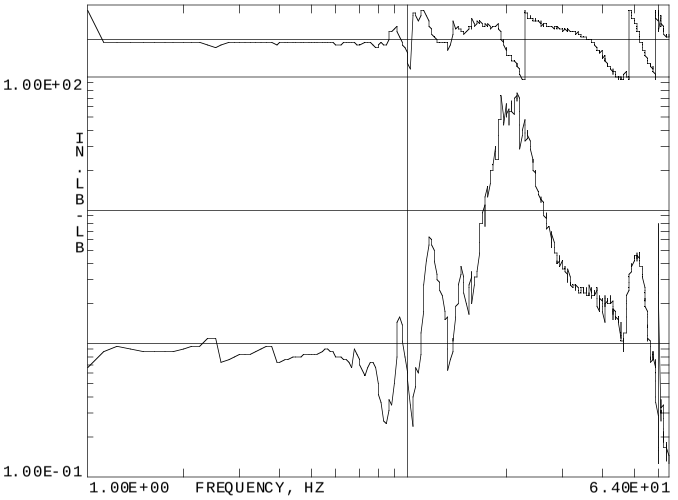

(h) Pitching moment response to lateral excitation.

Figure A-9. Concluded.

REPORT DOCUMENTATION PAGE

Form Approved
OMB No. 0704-0188

1. AGENCY USE ONLY *(Leave blank)*	2. REPORT DATE	3. REPORT TYPE AND DATES COVERED
	January 1994	Technical Memorandum

4. TITLE AND SUBTITLE

Shake Test Results of the MDHC Test Stand in the 40- by 80-Foot Wind Tunnel

5. FUNDING NUMBERS

505-59-36

6. AUTHOR(S)

Benton H. Lau and Randall Peterson

7. PERFORMING ORGANIZATION NAME(S) AND ADDRESS(ES)

Ames Research Center
Moffett Field, CA 94035-1000

8. PERFORMING ORGANIZATION REPORT NUMBER

A-94029

9. SPONSORING/MONITORING AGENCY NAME(S) AND ADDRESS(ES)

National Aeronautics and Space Administration
Washington, DC 20546-0001

10. SPONSORING/MONITORING AGENCY REPORT NUMBER

NASA TM-108801

11. SUPPLEMENTARY NOTES

Point of Contact: Benton H. Lau, Ames Research Center, MS T042, Moffett Field, CA 94035-1000
(415) 604-6714

12a. DISTRIBUTION/AVAILABILITY STATEMENT

Unclassified-Unlimited
Subject Category – 01

12b. DISTRIBUTION CODE

13. ABSTRACT ***(Maximum 200 words)***

A shake test was conducted to determine the modal properties of the MDHC (McDonnell Douglas Helicopter Company) test stand installed in the 40- by 80-Foot Wind Tunnel at Ames Research Center. The shake test was conducted for three wind-tunnel balance configurations with and without balance dampers, and with the snubber engagement to lock the balance frame. A hydraulic shaker was used to apply random excitation at the rotor hub in the longitudinal and lateral directions. A GenRad 2515 computer-aided test system computed the frequency response functions at the rotor hub and support struts. From these response functions, the modal properties, including the natural frequency, damping ratio, and mode shape were calculated. The critical modes with low damping ratios are identified as the test-stand second longitudinal mode for the dampers-off configuration, the test-stand yaw mode for the dampers-on configuration, and the test-stand first longitudinal mode for the balance-frame locked configuration.

14. SUBJECT TERMS

Modal damping, Structural frequency, Shake test

15. NUMBER OF PAGES

42

16. PRICE CODE

A03

17. SECURITY CLASSIFICATION OF REPORT	18. SECURITY CLASSIFICATION OF THIS PAGE	19. SECURITY CLASSIFICATION OF ABSTRACT	20. LIMITATION OF ABSTRACT
Unclassified	Unclassified		